FIRAT UNIVERSITY
GRADUATE SCHOOL OF NATURAL AND APPLIED SCIENCES
TÜRKIYE

EVALUATION OF THE EFFECTS OF EARTHQUAKES ON RADON AND TOTAL ELECTRON CONTENT VALUES AND METEOROLOGICAL CHANGES: A MONTE CARLO SIMULATION PREDICTION

Ahmet Sait ALALI

Master's Thesis

DEPARTMENT OF PHYSICS

Nuclear Physics

January 2022

FIRAT UNIVERSITY
GRADUATE SCHOOL OF NATURAL AND APPLIED SCIENCES
TÜRKIYE

Department of Physics

Master's Thesis

EVALUATION OF THE EFFECTS OF EARTHQUAKES ON RADON AND TOTAL ELECTRON CONTENT VALUES AND METEOROLOGICAL CHANGES: A MONTE CARLO SIMULATION PREDICTION

Author
Ahmet Sait ALALI

Supervisor Prof. Dr. Fatih KÜLAHCI

January 2022
ELAZIG

FIRAT UNIVERSITY
GRADUATE SCHOOL OF NATURAL AND APPLIED SCIENCES

T Ü R K I Y E

Department of Physics

Master's Thesis

Title:	Evaluation of the Effects of Earthquakes on Radon and Total Electron Content Values and Meteorological Changes: A Monte Carlo Simulation Prediction
Author:	Ahmet Sait ALALI
Submission Date:	21 December 2021
Defense Date:	25 January 2022

THESIS APPROVAL

This thesis, which was prepared according to the thesis writing rules of the Graduate School of Natural and Applied Sciences, Fırat University, was evaluated by the committee members who have signed the following signatures and was unanimously approved after the defense exam made open to the academic audience.

		Signature
Supervisor:	Prof.Dr. Fatih KÜLAHCI Firat University, Faculty of Science	Approved
Chair:	Assoc.Prof.Dr. Fethi DAĞDELEN Firat University, Faculty of Science	Approved
Member:	Assoc.Prof.Dr. Miraç KAMIŞLIOĞLU Bandırma 17 Eylul University, Faculty of Science	Approved

This thesis was approved by the Administrative Board of the Graduate School on
..... / ..... / 20.....

Signature

Prof.Dr. Kürşat Esat ALYAMAÇ
Director of the Graduate School

DECLARATION

I hereby declare that I wrote this Master's Thesis titled “Evaluation of the Effects of Earthquakes on Radon and Total Electron Content Values and Meteorological Changes: A Monte Carlo Simulation Prediction” in consistent with the thesis writing guide of the Graduate School of Natural and Applied Sciences, Firat University. I also declare that all information in it is correct, that I acted according to scientific ethics in producing and presenting the findings, cited all the references I used, express all institutions or organizations or persons who supported the thesis financially. I have never used the data and information I provide here to get a degree in any way.

25 January 2022

Ahmet Sait ALALI

PREFACE

In this study, general information about the Monte Carlo simulation was given by literature research and MATLAB was made. I would like to sincerely thank my dear advisor Prof Dr. Fatih KÜLAHCI, who guided him with his interest and suggestions at every stage of this study from the very beginning, and never withhold his financial and moral support, and I want to thank my family, who are my biggest supporters during this work.

Ahmet Sait ALALI

ELAZIG, 2022

TABLE OF CONTENTS

Page

ABSTRACT

Evaluation of the Effects of Earthquakes on Radon and Total Electron Content Values and Meteorological Changes: A Monte Carlo Simulation Prediction

Ahmet Sait ALALI

Master's Thesis

FIRAT UNIVERSITY
Graduate School of Natural and Applied Sciences

Department of Physics
January 2022, Page: xi + 60

An ARIMA and Monte Carlo simulation application are proposed to analyze the relationship of soil Rn-222 gas, ionospheric Total Electron Content (TEC) and some meteorological variables with earthquakes from theNorth Anatolian Fault Zone, Corum, Turkiye, one of the most active fault lines in the world. With the obtained results, statistically significant results are obtained for Earthquake-Radon gas changes and Seismo-Ionospheric Coupling. In addition, predictions were made and interpreted for future dates with unknown Rngas concentrations. We think that this study will be an important step for further studies on earthquake prediction.

Keywords: Radon; Total Electron Content; Meteorology; Foresight; Estimation; Monte Carlo; ARIMA; North Anatolian Fault Line

ÖZET

Depremlerin Radon ve Toplam Elektron İçeriği Değerleri ve Meteorolojik Değişimler Üzerindeki Etkilerinin Değerlendirilmesi: Bir Monte Carlo Simülasyonu Kestirimi

Ahmet Sait ALALI

Yüksek Lisans Tezi

FIRAT ÜNIVERSITESI
Fen Bilimleri Enstitüsü

Fizik Anabilim Dalı
Ocak 2022, Sayfa: xi + 60

Dünyanın en aktif fay hatlarından biri plan Kuzey Anadolu Fay Zonu, Çorum, Türkiye üzerinde tespit edilen toprak Rn-222 gazı, iyonosferik Toplam Elektron İçeriği (TEİ) ve bazı meteorolojik değişkenlerin depremlerle olan ilişkilerini analiz etmek için bir ARIMA ve Monte Carlo Simülasyonu uygulaması önerildi. Elde edilen sonuçlar ile Deprem-Radon gazı değişimleri ve Sismo-İyonosferik Çiftlenim için istatistiksel olarak anlamlı sonuçlar elde edildi. Ayrıca, Rn gazı derişim değerleri bilinmeyen ileri tarihler için öngörüler yapıldı ve yorumlandı. Bu çalışmanın deprem kestirimi üzerine olacak ileri çalışmalar için önemli bir adım olacağını düşünmekteyiz.

Anahtar Kelimeler: Radon; Toplam Elektron İçeriği; Meteoroloji; Öngörü; Kestirim; Monte Carlo; ARIMA; Kuzey Anadolu Fay Hattı

LIST OF FIGURES

Page

LIST OF TABLES

Page

SYMBOLS AND ABBREVIATIONS

Symbols

^{222}Rn	: Radon gas
^{238}U	: Uranium
M_w	: Moment magnitude
M_b	: Body wave magnitude
M_s	: Surface wave magnitude
M_L	: Local magnitude
foF2	: Critical frequency
foEs	: Sporadic frequency
CO2	: Carbon dioxide
CH4	: Methane
H2	: Hydrogen
Sb	: Antimony
As	: Arsenic
Hg	: Mercury
Pb	: Lead
α	: Alpha particles
β	: Beta particles
γ	: Gamma rays
Bq	: Becquerel
Ci	: Curies
kJ	: Kilojoule
NaI	: Sodium Iodide
ns	: Porosity
τ	: Tortuosity
De	: Diffusion coefficient parameter
kr	: Permeability
η	: Viscosity
μ	: Mean
σ	: Standard deviation
Kp	: Disturbance of the Earth's magnetic field caused by the solar wind
ϕ	: Coefficients of autoregressive
θ	: Coefficients of moving average

Abbreviations

TEC	: Total Electron Content
GPS	: Global Positioning System
NAFZ	: North Anatolian Fault Zone
A.D.	: Anno Domini
B.C.	: Before Christ
CPB	: Convergent Plate Boundary
DCB	: Divergent Plate Boundary
TPB	: Transform Plate Boundary
P-wave	: Primary Waves

1. INTRODUCTION

Rn-222 is generated due to nuclear decay of the crustal radium (Ra-226) and uranium (U-238). Rn-222 has the longest half-life (3.82 days), is chemically uncertain and has omnipresent occurrences. Radon gas travels over greater distance on the surface of the Earth through different means. Such as diffusion, convection or advection through concentration and external power, such as pressure gradients [1–2]. If soils with a lower permeability are the medium composition, the diffusion phase prevails, while convective transport is dominant for soils with higher [3]. Many researchers have noted Rn-222 levels increase from a few hours to several weeks [4–13] in Taiwan in fault zones before earthquakes occur, [14] Radon variations have been predicted as a valuable method to classify earthquake precursors in Japan [15] in Marmara, Turkey [14] in Western Turkey [16]. Similar radon abnormalities were found in India a couple of days before earthquakes [17–27]. Examined worldwide land, water, and air radon analysis and confirmed that radon is a reliable predictor of the prediction of earthquakes in the future [28].

Researchers have attempted to explain the preparatory physics earthquakes. For example, phase expansion was studied and presented by [29], the model for stress corrosion by [30], the model for the system of compression by [31] and the model for Asperity by [32]. Both these four think tanks postulate shifts in the radon level as the pressure Earth modifications occur during the planning of the earthquake. Radon is also affected by tectonic activities, meteorological parameters, for example, temperature, pressure and wind speed, precipitation and humidity. The radon is also affected by seasonal variations. The impact of these parameters on radonemission dynamics ranges between several hours and several days [10, 33–36, 38–41]. Seasonal variations include diurnally, semi-diurnally and seasonally occurring periodicities; their effects exist in the soil radon signal as periodic or almost periodic components [42]. Given the intra-linearand non-stationary aspects of radon emissions from the field, multiple signal processing techniquessuch as main component analysis [11], spectral degradation [44] and single spectrum analysis, etc. [45] have limits when the radon signal is isolated from the periodic noise. A two-step decomposition procedure has been introduced [46] for the efficient separation of periodic signal components, namely, the Hilbert-Huang Transform based on empiric mode decomposition (EMD)(HHT). A brevity definition can be found in [46–47] of this EMD system. In a broad range of test fields, this approach has been widely applied, beginning with plasma physics [47–48], structural engineering [49–50], medical research [46–52] in the Earth sciences [14, 54–55] in the Northampton English East Midlands [53] in the Marmara area, which is seismically active [56]. The Hilbert Huang Transform (HHT) method based on EMD used in the soil radon time series in western Bengal and [57] Himalayan Sikkim area in Ravangla and detected major irregularities before the earthquakes in the respective regions.

2. LITERATURE REVIEW

2.1. History of radiation

Radiation is the emission or transmission of energy in the form of electromagnetic waves or particles. This also include "radioactive materials emitting rays such as alpha, beta, gamma" or "all the elements that make up any electromagnetic beam emitted in space." If the number of neutrons in the atomic nucleus of a substance is considerably higher or lower than the number of protons; Such substances show an unstable structure and the neutrons in their nuclei are broken down by emitting various rays such as α, β, and γ. Substances that are broken down by radiating rays in their surroundings in this way are called radioactive materials. In 1896, the French physicist Henri Becquerel first noticed that uranium salt emitted invisible rays. Two years later, Marie Curie and her husband Pierre Curie encountered similar rays while experimenting with uranium. In this experiment, they saw that polonium and radium were formed, and they were the first to discover these two elements [37].

2.2. Examples of background dose

The radiation in the background is different according to place and time and examples are given in the Table 2.1 below:

Table 2.1. Average annual human susceptibility in milliSieverts (mSv) to ionizing radiation per year.

Average yearly ionizing radiation exposures of humans in milli Sieverts (mSv)				
Radiation source	**World [43]**	**The US[53]**	**Japan [58]**	**Remark**
Air	1.26	2.28	0.40	Depends primarily on indoor deposition from radon
Food - water	0.29	0.28	0.40	(^{40}K, ^{14}C, etc.)
Terrestrial radiation	0.48	0.21	0.40	Depends on soil and materials of construction
Cosmic radiation	0.39	0.33	0.30	altitude depends
Subtotal(natural)	2.40	3.10	1.50	Relevant populations earn 10–20 mSv
Medical	0.60	3.00	2.30	Radiation therapy is excluded from the worldwide statistic, with U.S.
Consumer items	–	0.13		Alcohol, air transport, supplies for construction, etc.
Nuclear testing	0.005	–	0.01	1963 height 0.11 mSv and after it decreased; higher close to sites
Occupational exposure	0.005	0.005	0.01	Worldwide averages for staff are just 0.7 mSv, mostlydue to the use of radon in mines.
Chernobyl	0.002	–	0.01	0.04 mSv peak in 1986, decreasing since; nearer site higher.
Nuclear fuel cycle	0.0002		0.001	Excludes workplace exposure up to 0.02 mSv near sites;
Other	–	0.003		Industrial, safety and healthcare, education and science
Subtotal (artificial)		0.61	3.14	2.33	
Total		3.01	6.24	3.83	**milli Sieverts per year**

2.3. Environmental Radon and Radium

The radium and radon contribution to ambient radioactivity is significant. The decay of radioactive elements in the soil cause radon to occur naturally in the atmosphere and can accumulate in houses constructed in regions where such a decay had occurred. It is projected that 2% of all cancer deaths in Europe are caused by radon [59]. Like radon, radium is a toxic ingredient that is life threatening. It can be harmful if the dose goes above 20–50 mSv/year.

2.4. Radium Radiation in the oil and gas sector.

Radium with its daughters also contain traces in the oil and gas industry. The oil well sulfate scale can be rich in radium. Water in a petroleum field is also roguish although seawater is sulfate rich with strontium, barium and radium, thus radium can be formed by the barium/strontium sulfate, which is a precipitate carrying water, whether released in the sea or combination with the sea water fromthe oil well [61]. There is no unexplained local radiation due to incorrectly removed radium-based radio-luminescent paints. [62]

2.5. In Radioactive Quackery

Eben Byers was a American who founded of radium in 1932; leading to the use of a toxic Quackery substance called the Radithor. About 1 μCi (40 kBq) of ^{226}Ras and 1 μCi was found in the radiator per bottle of ^{228}Ra. Radithor has a long biochemicalhalf-life in bone, becoming a calcium representation from the mouth and radium [63].

2.6. Radon

Figure 2.1. Air radon is part of the background radiation that can be seen in a cloud chamber [64].

The decay of ^{218}Po and ^{214}Pb, daughters of ^{222}Rn, is causing the bulk of dosage. The skin and lungs' nuclear dosage should be reduced by at least 90% when the daughters are exposed. This

should be done this with a mask and a costume for protecting the whole body. Radon radiation gives raise to the damaging impact of radon at the same time as Rn and Rn daughters (Figure 2.1). Radon has shown more carcinogenic in uranium mines in smokers than in nonsmokers[64].

2.6.1. The history and etymology of Radon

Radon was discovered in 1899 as the fifth radioactive element at the University of McGill by Ernest Rutherford and Robert B. Owens [110–113]. Rutherford found that thorium compounds Emit toxic gas continuously which stays a few minutes in radioactive, which he called "emanation" (Emanare, flow from the Latin, emanation) [114] and subsequently "thorium emanation" ("Th Em"). Friedrich Ernst Dorn experimented in 1900 that showed Ra compounds emanate from a "radium emanation" radioactive gas ("Ra Em") [115–116]. In 1901, the radioactive emanations of Rutherford and Harriet Brooks were proved but Curies were credited with discovering this element [117]. André Louis Debierne watched it in 1903 analogous Actinium emanations [118–119] and named actinium emanation ("Ac Em"). For the three emissions of ex-radio, exthorio, and exactlyinio in 1904, some shortened nameswere quickly suggested; [123] In 1918 radium (Ra) and thoron; and in 1919 radium, thoron, Actinon (Ac), [110] Rn and, in 1920, ultimately radon, thoron, and actinone [120–124]. The name Rn is notrelated to Johann Radon's name, an Austrian mathematician. Sir William Ramsay suggested that, in 1905, the 'emanations′ contain a new component of a noble gas family, because the spectrum of these three gases is similar to the molecular inertia of argon, krypton, and xenon [123].

In early twentieth century, the ^{210}Pb radon girl entered the gem industry inAmerica. This was the gold seed, comprising ^{222}Rn, which was melted down after the decay of theradon [124–125]. Ramsay and Robert Whytlaw-Gray calculated the melting temperature and approximate density in 1909 (Figure 2.2). In 1910, it was the heaviest gas known. In 1910, 'The term radium emanation,' they proposed the name niton as well [126-127]. "Radium emanation," to emphasize the proprietorship of radiology. The International Atomic Weights Commission approved, which was accepted in 1912 [117]. The Committee for Chemical Elections and the Pure and Applied International Chemical Union in 1923 (IUPAC) Rn, Tn and An. The producteventually took the name the most stable isotope, radon, as it was counted rather than called, whileTn's name was ^{220}Rn and An's name was changed to ^{219}Rn, which added some doubt to the literarydiscovering of that element, as Dorn's found radon as the isotope, but he was not the first to detectradon [128]. The factor was also just called emanation in the late 1960s [129]. In 1962, radon fluoride was the first synthesized drug. Meanwhile, the term radon is still used as the name of ^{220}Rn to reduce this misunderstanding either with the element or its isotope ^{222}Rn [130]. The term actinon for ^{219}Rn is unusual today, possibly for a short half-life [128]. We have recognized for a long time the threat of

radon emissions of mines of exposures of 1,000,000 Bq/m^3. In 1530 Paracelsus identified a waste of mining disease, mala metallorum, and the ventilation in mines suggested by Georg Agricola to help prevent mountain disease (Bergsucht).Their study of miners from Schneeberg, Germany [131] found this disease to be lung cancer by Harting and Hesse in 1879. In the Joachimsthal area of Bohemia, radon and wellbeing were the first major experiments of uranium mining [132]. Uranium miners in the Southwest USA were working during the early cold war in the US with only decades of health consequences and research and mitigation; regulations were adopted only in 1971 [133]. As soon as 1950 it was recorded that radon was present in indoor air. Study on indoor radoncauses, concentration determinants, health impacts and prevention methods were started at the startof the 1970s. Following a highly reported event in 1984, the phenomenon of indoor radon was widely publicized and investigated more intensively in the US. A worker was discovered to be polluted with radioactivity Pennsylvania nuclear power plant during scheduled testing. A high levelof radon was then classified as responsible in his household.

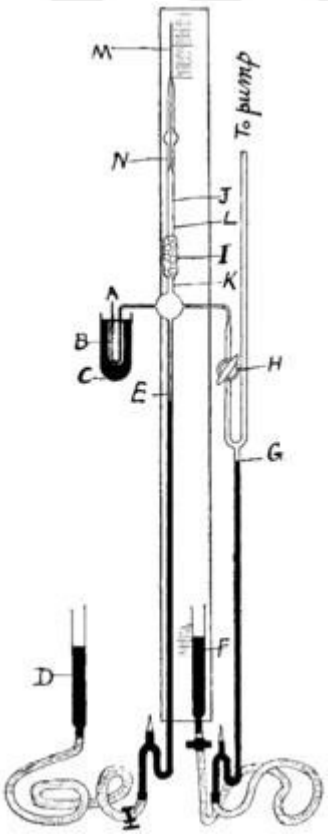

Figure 2.2. Ramsay and Whytlaw-Gray equipment used for Rn isolation [126].

2.6.2. Occurrence

Open-air radon concentration ranges from 1 to 100 Bq/m^2 [64–65], radon is also inherent in spring waters and hot springs [56, 66]. Radium springs emit radon and in Misasa, Japan, Bad Kreuznach, Germany, are richer in radium. Radon naturally exhausts from the earth, particularly in some areas, but not just areas with granitic soils. Rn is a radium progeny, which in turn is a declining uranium product (Figure 2.3). A visualization of the estimated radon levels can be acquired in houses to further prepare for home radon reduction [67]. Note that while high uranium does not necessarily correspond to a high levelof radon in air in the ground/rock below a building, a positive association can be found between soil uranium content and radon level in the air.

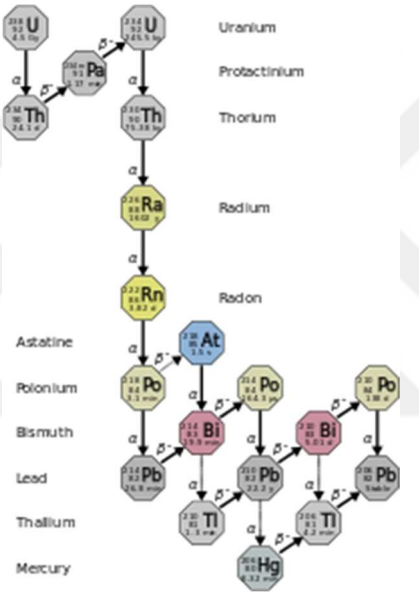

Figure 2.3. The series of radium or uranium [67].

2.6.3. In the air

The consistency of indoor air is connected with radon, which plagues many households. (see "Houses Radon" in Figure below). Radon (^{222}Rn) emitted into the air can be measured at ^{210}Pb and other radioisotopes and ^{210}Pb. The deposition rate of this radioisotope is highly seasonal. It is important to remember. The deposition rate in Japan is seen in this chart [68].

2.6.4. In groundwater

Radon is also present in water, especially in ponds, and springs. Water circulation in buildings, often in the form of tap water or well water used for daily use can also be a source of

Radon. Radon may penetrate the environment to become a means of human exposure, or human beings can drink water, that is another route of exposure (Figure 2.4) [69].

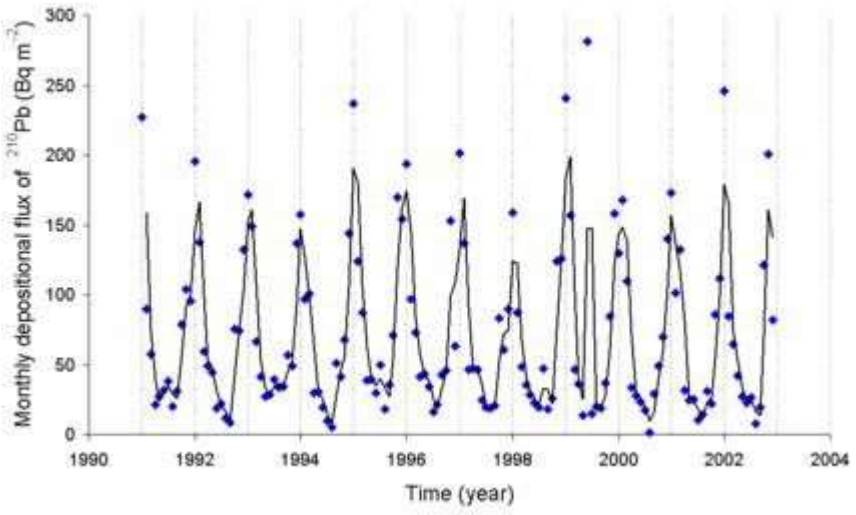

Figure 2.4. Japan Deposition levels of lead-210 according to the time in Japan [69].

2.6.5. Radon in rainwater

Atmospheric processes can lead to Radon taking part in cloud formation process, which leads to its presence in clouds and storms [70-71]. Estimates of rain fall age is derived from the calculation short-lived progeny of radon decline isotopic concentration in rainwater [72].

2.6.6. The oil and gas sector

Water, oil and gas from a well also contain radon. The Rn deteriorates into solid radioisotopes, forming coverings within the piping. The section of the plant where propane is stored in an oil refining plant is also one of the most polluted locations, as radon has the same cooking point as propane [73].

2.6.7. In mines

Since uranium minerals release radon and their radioactive daughter components, the mining of uranium is significantly more hazardous than other hard rock mining systems (which are also dangerous), therefore mines need proper ventilation systems. In the fifties,a substantial number of Navajo Indians became US uranium miners, when several Navajo reservations found uranium mines. Since Uranium and radon-222 toxicity a statistically important group of these miners eventually developed small-cell lung cancer that is normally unlinked to smoking and a normal decay agent of uranium [74]. The radon emitted by Uranium has been shown to not be the uranium itself as the cancer-causing agent [75] in 1990, Radiation Exposure CoverageAct compensation has

been given received to patients and their descendants. At a workplace the amount of Radon could bemanaged by drainage, the audience can screen and the water inside the mine can be controlled. When a mine is dropped, the level in a mine will rise to a level that will make the skin red (a mild radiation burn). Radon concentration can reach between 400 and 700 kBq m^{-3} in some mines [76-77].

2.6.8. Radon in Homes

Due to the 1984 situation of Stanley Watras, a Nuclear Station in Limerick employee in Pennsylvania, the threat of radon radiation in homes gained a broader generalrecognition after 1984 [78-79]. In his two-weeks straight to work, Watras sent radiation warnings(see the Geiger counter) while the authorities were searching for the pollution caused. The origins of radon shocked them in its basement was amazingly high and that it was not associated with the nuclear power station. It has been determined that the dangers associated with staying in your home amount to 135 packs of cigarettes per day [80]. Rn can accumulate in cellars and buildings, depending on how houses are constructed and ventilated. The European Union [81] recommends mitigation from the 400 Bq/m^3 concentrations of the old house and 200 Bq/m^3 for the next households. For households with concentrations of more than 8 pCi/l (300 Bq/m^3), Steps are advised by the National Radiation and Measurement Council (NCRP). The US General Surgeon and the EPA prescribe radon tests in all households. Millions of homes Radon was screened in the United States since 1985 [81]. The degree of radon in the building can be reduced by adding a creeping field in the ground floor, subject to forced ventilation. [82]

2.6.9. Radon Physical properties

Radon is a colorless, odorless, and tasteless gas [83] and cannot be found isolated by humans. Radon forms a monatomic gas at normal temperatures and pressures. It has a density of 9.73 kg/m^3, which is about eight times atmospheric density (1.217 kg/m^3) at sea level [83–84]. Radon emanates dazzling radio light, which transforms yellow to orange-rod, as its freezing temperature decreases, from 202 K (−71 °C; −96 °F) [85]. When concentrated,intensive radiation emitted by radon glows [86]. The report was published in French. Sparely water-soluble, radon is Lighter gasses more soluble than noble. In organic fluids, radon is significantly more soluble than water. Which is the equation of radon solubility, [87] the absolute temperature and solvent constants are the molar radon fraction (Figure 2.5).

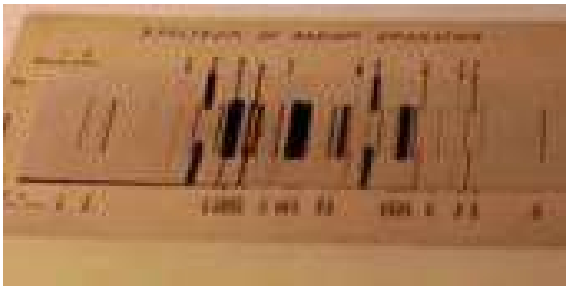

Figure 2.5. Spectrum of emissions of Rn taken in 1908 by Ernest Rutherford [83].

2.6.10. Radon Chemical properties

Radon is not chemically reactive, it has zero valence electron, considered (family of the noble gasses). Radon-222's 3.8-day half-life gives it a perfect tracer in physical sciences. Radon is a gas under normal conditions [88]. Its outermost shell contains 8 electrons, and Inert of most naturally occurring chemical reactions, including combustion. The outer electrons are thus closely bound in a stable, minimal energy configuration [89]. The energy for its first ionization is minimum energy 1037 kJ/mole to detach an electron from it [90]. Radon is less electron-negative than the material one time before, Xenon, in line with normal patterns, and thus more reactive. Early research showed that radon hydroxide stability could be the same as the chlorine or sulfur dioxide hydrates (Cl_2) (SO_2), and substantially better than the stability of hydrogen sulfide (H_2S) [91]. Experimental chemical analysis of radon is seldom performed due to their expense and radioactivity, and therefore there are relatively few known radon compounds, Fluorides or oxides. Radon can be rusty by strong oxidants, including fluorine and hence difluoride of radon (RnF_2). Water may also be converted to fluoride hydrogen and radon gas in the form of water, [92–93] decomposes at temperatures above 523 kg (250 °C; 482 °F) down to its components [94]. The uncertainty is poor and was considered RnF_2. The compound could not be analyzed in-depth due to short radon half-lives and metabolite radioactivity. Theoretical tests of this molecule forecast a bond gap Rn–F of 2.08-angstrom (Å), which is Stabilized and lower reactive xenon difluoride thermodynamically than its lightweight counterparts (XeF_2) [95]. An even reduced enthalpy of formation was expected to octahedral molecule RnF_6 than the difluoride [96]. By the following reaction the $[RnF]^+$ ion is expected to form [88, 97]:

$$Rn\ (g) + 2\ [O_2]^+\ [SbF_6]^-\ (s) \rightarrow [RnF]^+\ [Sb_2F_{11}]^-\ (s) + 2\ O_2\ (g) \qquad (2.1)$$

Radium decay in radium halides is a response that is used to reduce the radon level escaping from goals of radiation, which may contribute to the forming of radium compounds. Besides, SbF^6, TaF^{-6}, and BiF^{-6} anions contain salts from the $[RnF]^+$ cation. At 173 K (−100°C, −148°F), radonis

also oxidized to RnF_2 by dioxygen difluoride [92]. Among the few other known radon compounds, radon oxides are only confirmed [98] in thetrioxide (RnO_3) [99]. The higher fluorides RnF_4 and RnF_6 are claimed [99], but it is unclear if theyhave yet to be synthesized, [100] and are calculated to be stable [99]. Experiments of undisclosed radon-confining materials dissolved along with xenon hexafluoride may have detected these compounds as RnF_4, RnF_6 or both [92]. Radon trace heating was asserted to generate higher fluorides, which hydrolyzed to form the RnO_3, Pentfluoride bromine and sodium fluoride or nickel fluoride, and Xenon, Fluoride. While these arguments had been argued that radon was also attributed to precipitation as solid complex $[RnF]^{+2}[NiF6]^{-2}$, it was taken as evidence the co- promotes radon were produced from aquatic solution with $CsXeO_3F$ through further analyses of the hydrolysate solution. The high fluoride concentration used may have arisen from the $[RnO_3F]^-$unestablished in other studies. Electro migration experiments also indicate the existence by analysisof the homologous xenon trioxide The poor acid (pH>5) solution includes cationic $[HRnO_3]^+$ and anionic $[HRnO_4]^-$ radon [99].

It is possible that due to the heavy iconicity and high positive radon load of RnF^+ radon difluoride (RnF2), the difficulties of determining higher fluorides of radon result kinetically from oxidation outside the divalent state. RnF_2 molecules will require spatial separation, to identify considerably higher fluorides, RnF4 of which is predicted to occur. Therefore, while RnF_4 should be close to the xenon tetrafluoride (XeF_4), RnF_6 is possibly far from Xenon hexafluoride less stable (XeF_6): even radon hexafluoride is probably a normal octahedral molecule because of the inert pair effect, as opposed to the twisted octahedral form of XeF_6 [92, 101–102].

The prediction of radon carbonyl (RnCO) is stable and linear molecular geometry [103]. Spin-orbit connecting has shown that Rn_2 and RnXe molecules are considerably stabilized [104]. As a tumor medicine, the Radon is suggested caged inside a fullerene [105–106]. Perradonate of barium (Ba_2RnO_6), similar to perxenate of barium, is expected to be the most stable Rn (VIII) compound. Rn (VIII instability)' s is caused by the relativistic stability of the 6s casing, called the inert pair effect [100].

Non-reactive Rn is presented as RnF^+ and Rn_2^+; add up to the RnF^{-3} and RnF_2^{-4} complexes parallel with beryllium (II) and alumina chemistry are formed in a solution of halogen fluoride (III) [92]. The $Rn^{2+/}$Rn pair's normal electrode potential has been measured at 2.0 V, even though the aggregation of a watery solution of stable radon ions or compounds is not shown [92]. No stable isotopes are found in radon.39 radioactive isotopes with atomic masses of between 193 and 231 were characterized. [107-108]. ^{222}Rn is the most stable isotope, representing a decay product of ^{238}U, ^{226}Ra. [109].

2.7. Applications of Radon

2.7.1. Medical

The cure of illnesses in radiothorium was in the early 20th century [135].The patients were subjected to radon for their 'medicinal effects in a small, enclosed space. The carcinogenic value of radon was subsequently seen by its ionizing radiation. The dangerous radio activeness of Radon's molecule has not increased the health of cells, but it has also been used to destroy cancer cells [136]. Radon therapy was proposed in a method used to mitigate autoimmune disorders like arthritisas radiation hormesis [137]. As a consequence, the "Health Mining" developed in Basin, Montana,at the beginning of the 20th century attracted people seeking healthcare relief such as arthritis by limiting radioactive mineral water and radon radiation. The procedure is prohibited because high doses of radiation have well-documented health effects [138]. Radon is used for treating tumors, known as brachytherapy in implantable seed, of gold or glass. Goldseeds were created by the supply of radium by filling a large tube of radon and then by squeezing and cutting the tube into small sections. The first short-lived elements of the radon and gamma raysare formed (^{218}Po, ^{214}Pb, ^{214}Bi, ^{214}Po) [136]. The seed is left for radon and the first decay product, which are short-lived. Radon radiationis up to 1/2 000 of the initial amount after 12 half-lives (43 days). Radon decay product ^{210}Pb, the primary occurrence in the residual region of which is 2.000 times the half-life of radon (22.3 years),and its successors ^{210}Bi and ^{210}Po are the radon decay product ^{210}Pb, with its 1/2.000 of radon activity.

2.7.2. Scientific

The emanation of radon from the soil varies by the type of soil and by surface level, while outdoor levels may be used in a restricted way to detect air masses. Atmospheric scientists have used this fact. Radon is being used in hydrology, which studies the relationship between groundwater and waterways, because of the gradual loss of air and comparatively fast decay. Experimentally, soil radon concentrations are used to chart submerged geological defects atthe surface because of the accumulation of defects [139]. Likewise, the application of geothermal gradient prospective was somewhat restricted [140]. Researchers have examined Radon anomalies in earthquake prediction ratios in groundwater radon [141–143]. An increasing radon accumulation has been speculated by the generation of new underground splits, allowing an expanded exchange of groundwater and radon split. Newer fractures could not be believed to lead to serious earthquakes unreasonably. In the 1970s and 1980s, scientific radon emission tests demonstrated that sometimes no radon signal existed during earthquakes, and sometimes radon were detected without an earthquake. Many of them rejected it as an untrustworthy metric. As a potential successor to NASA,

it was studied in 2009 [144].

Radon is a contaminant that is released from geothermal power plants when it is in the deep underground-pumping material. It spreads easily and in numerous experiments, no radiological threat was shown. Furthermore, conventional Systems re-inject the deeper material into the atmosphere instead of pouring it into the ground [145]. In the 1940s and 1950s, radon was used for commercial X-rays [146–147]. Additional formsof X-ray used in this application were quickly replaced by radon during the Second World War, asthe cost was smaller and alpha radiation was less possible.

2.8. Radon measurement techniques

Radon can be measured directly and indirectly detected by its descendants in two ways. Radon identification and calculation can be achieved by detecting α, β, or μ. Each identification method can be used: atomic solid skin, gamma spectroscopy, emulsion, and adsorption. Beta-watching, Ionization chambers, surface boundary sensors. SSNTD, electrometer or electroscope; light-emitting phosphor, electrode, and set. Thermostat-sensitive phosphorus. Radon-22, which involves the pushing of gas into or through a detector system, can be determinedby a passive approach by diffusion only or action while approaching measurement volume.

2.8.1. Passive equipment

The sensor is mounted in an opening vessel for the interaction with radon. The container is designed to hold the sensor and to allow a sensitive size region-wide enough to generate and track as many α-particles as shortly possible, as well as a plastic or paper inverted container in separate versions [148] for direct radiation measurements, or specialized bin.

2.8.2. Active devices

Many devices may be transformed into active devices by using a fan or a pump [149]. Installed the detector from which radon is propelled from the earth. The gas drift pushes to the outside of the instrument electronic measurement. The accumulation of radon is then measured. Radon level can also be detected by direct scintillation by pressing air through the sensor [150]. Radon or extractsamples are the second methods of active detection. Following the sampling, the radon-containingwater or air or the solution is detected at the laboratory. The techniques of sampling are different, but all of them must take special care not to pollute the study. Syringes, compressors, vacuum containers, water sampling, spot degas, pump suction, etc. may be used for sampling.

2.9. Radon Transport

2.9.1. Emanation

Radon atoms are emanated from a material which contains its mother nuclide (Radium atoms). The emanation rate of radon has been stated to be affected by soil quality and many environmental factors [151-152]. The effect of the re-adsorption of Rn on pore surfaces is reduced if the moisturecontent is limited; however, the release of Rn increases marginally, to a certain level of humidity above which radon release decreased again due to the lower diffusion rate of pores [153]. Radon emission from soil depends not only on the concentration of ^{238}U and ^{226}Ra butalso on the essence of host mineralogy and host rock and soil permeability. The result was observedto decrease the Rn emanation from brick surfaces, by reducing the density of radon within the brick [154].

2.9.2. Diffusion

Diffusion is the main process by which radon is transported into and out of the basement modules and seems largely unchanged from isolating vapor retardants and components. Radon instability and differential pressure gradients associations; was found to be linked to the air current in block walls and soil that disrupted the spread of radon to the inside. Radon is carried by absorption, Mechanical and convective streaming, percolation of rainwater, and ground-water flow to meet air or water carrying radiation particulate matter. It has been shown that the pressure mechanism is inadequate to be the dominant radon penetration mechanism in the houses, and the modification of gas flows in clay and concrete will surpass the pressure-driven flow significantly [155].

2.9.3. Flux from the soil

The Rn emission and exhalation concentrations in the soil vary from place to place because of variations in soil composition, porosity, permeability, and grain dimensions. The soil's humidity content is determined by the amount of water in the soil as part of the dry weight of the solids that form the soil matrix [156–157].

$$\%\ Soil\ watercontent = \frac{Mass\ of\ soil\ water}{Mass\ of\ dry\ soil\ solids} x100 = \frac{W_1 - W_2}{W_2} x100 \qquad (2.2)$$

The masses of the wet and dry samples are W_1 and W_2. The porosity p of a porous material is the calculation of the total pore area which can beoccupied and expressed as a percentage of

the water in that material [156]

$$Porosity = \frac{V_W - Vd}{V_W} x100,\ \mathrm{V_d} = \frac{Weight\ of\ dry\ sample}{Denstiy\ of\ soil\ grain} x100 \tag{2.3}$$

where the amount of dry and wet specimen is V_d and V_w:

VD = dry sample weight Soil Crop Density, VD = dry sample weight Soil Crop Density [156].

The radon diffusion equation is shown, assuming that the medium is source-free

$$\frac{D_e}{P}\frac{\partial^2 C}{\partial x^2} - \lambda C = 0 \tag{2.4}$$

where C is the concentration of the gas, λ is the decay constant of the gas in s^{-1}, D_e is the coefficient of effective diffusion of porous $cm^2\ s^{-1}$ steam, and the medium p is of porosity.

The solution of Eq. (2.4) is

$$C(x) = C(0)\exp(-\sqrt{\frac{\lambda P}{D_e}}) \tag{2.5}$$

where C(x) is the radon concentration at a distance x at any moment, C_o is radon concentration in the spring and $D_e = D - p$ where D is the coefficient of diffusion. Relationships are complex between radon levels in the soil and indoor radon concentrations. However, soil radon concentration data are the starting point for the evaluation of the anticipated radon in the building built. The most important radon flux soil parameters at the top of the crack are effective diffusion coefficients, soil gas permeability and low radon level of the soil [158–159]. The accumulation of radon from an infinite column is determined by the distance z to the soil [160].

$$C(z) = C_\infty(1 - \exp(-\frac{\lambda z}{d}) \tag{2.6}$$

where, λ is the decay constant; d is the diffusion constant; and C_∞ is the infinite depth concentration.

2.10. Atmosphere

The Earth's atmosphere is the layer of gasses (termed air), maintained by the gravity of the Earth, which encircles and form the Planet Earth's planets. The Earth's atmosphere preserves life on Earth by causing friction to allow fluid water to survive on the top of the planet. By length, 78.09% nitrogen, 20.95% oxygen, argon of 0.93%, carbon of 0.04%, and a limitednumber of other gasses can be found in dry air [161]. Air also contains variable vapor levels, on average at sea level

about 1 percent and in the whole atmosphere 0.4 percent. The atmospheric structure, Altitude differs in temperature except for pressure and only in the troposphere of the Earth and artifice atmospheres is the environment appropriate to be seen in terrestrial photosynthesis plant and terrestrial breathing of animals [162].

The Great Oxidation Event Human beings have also led to major changes in air quality atmosphere structure, especially after industrialization, leading to dramatic changes in the environment, Ozone degradation, and warming of the atmosphere. The weight of the atmosphere is between 5.15 and 1018 kg (6.8 miles), of which 3 quarters are within approximately 11 km (6,000 ft.). With the altitude and no established border between the atmosphere and outside space, the atmosphere gets thinner and thinner. Due to features such astemperature and structure, several layers can be differentiated in the atmosphere. The atmospheric research and the mechanisms of the Earth are referred to as aerology and covers various subfields, excluding atmospheric mechanics and climate science. Richard Assmann and Léon Teisserenc de Bort are early pioneers in this area [163].

2.10.1. Ionosphere

The Earth's ionized part [164–165] is 48 kilometers (30 miles) to an altitude of 965 kilometers [166], including the thermosphere, the part of mesospheric and the part of Exosphere [167]. Solar radiation is ionizing in the ionosphere. In air energy, has a major function and shapes the magnetosphere's inner edge. Practical value because it affects the dissemination of radio to remote areas of the world, among other features [167] (Figure 2.6).

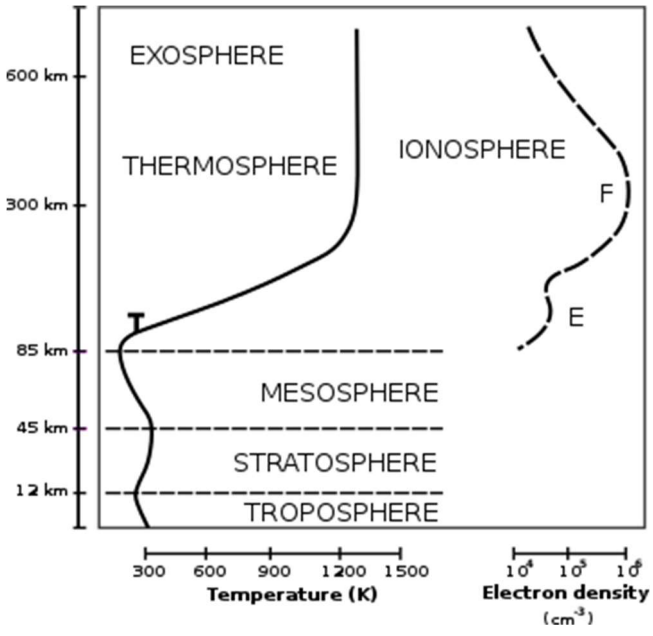

Figure 2.6. Relationship of the atmosphere and ionosphere [167].

Back in 1839 Carl Friedrich Gauss, a German mathematician and physicist, had suggested that an atmosphere electrically conducive area would account for observable changes in the Earth's magnet field. Guglielmo Marconi had a kite-supported antenna at 152.4 m (500 ft.) to receive the first signal trans-Atlantic. A spark-gap transmitter was used by the Poldhu station transmission (Cornwall) to deliver a signal at Around 500 kHz and 100 times as powerful as any other radio signal. The Morse letter S code is 3 times the message received. The signal can bounce off the ionosphere twice to arrive in Newfoundland. However, based on analytical and experimental work, Dr. Jack Belrose disputed this. However, one year later in Glace Bay, Nova Scotia, Marconi accomplished transatlantic wireless contact [168]. The plan of Oliver Heaviside involved methods for sending the signals across the curvatureof the Earth. Arthur Edwin Kennelly also found in 1902 aspects of the ionosphere's radio electric properties. The term ionosphere was introduced in a letter only in Nature published in 1969 by theScottish physicist Robert Watson-Watt in 1926. We have seen the overwhelming acceptance of theword 'stratosphere' in recent years... And 'troposphere' accompanying words... The concept "ionosphere" seems to be an extension to this sequence in the area where the key feature is massiveionization with significant medium-free pathways.

In the early 1930s, Radio Luxembourg's test broadcasts unwittingly demonstrated the ionosphere had been modified for the first time using radios; HAARP performed several experiments with the Luxembourg effect in 2017 [169]. A study of the ionosphere started with the Canadian satellite Alouette 1 in 1962. Alouette 2in 1965 and two satellites ISIS in 1969 and 1971 were successful, followed in 1972 and 1975 by AEROS-A and -B, both for ionosphere measurement. The first Syncom 2 geosynchronous operational satellite was launched on July 26, 1963. [170] The siting board of radio beacons and measurements permitted by its predecessors, on the radio beam of the geostationary orbit to the earth receiver, of the total electron content (TEC) variation for the first time. (TEC is evaluated specifically after the polarization plane rotation.) Elizabeth Essex-Cohen, an Australian geophysicist, was using to track Australia and Antarctica since 1969 [171]. In 1959, the soil was disturbed on the first ISR site in Arecibo, Puerto Rico. There are 15 such pages when they are published. Many of these pages and other related details are shown in Table 2.2.

Table 2.2. Related Coordinates and Parameters

Observatory	Frequency (MHz)	Geographic Latitude	Geographic Longitude	L	UT-LT
Jicamarca, Peru	49.9	11.9^0S	76^0W	1.05	5
Altair, Kwajalein	155.5	8.8^0N	167.5^0E	1.1	−11
MU, Japan	46.5	34.85^0N	136.10^0E	1.33	−9
Arecibo, Puerto Rico	430	18.3^0N	66.75^0W	1.43	4
St.Santin, France*	935	44.6^0N	2.2^0E	1.76	0
Millstone Hill, Massachusetts	440	42.6^0N	71.5^0W	3.12	5
Chatanika, Alaska*	1290	64.9^0N	147.7^0W	5.51	10
Poker Flat ISR (PFISR)	450	64.9^0N	147.7^0W	5.51	10
EISCAT (Tromso Norway)	224/933	69.6^0N	19.2^0E	6.3	−2
Sondre Stromfiord, Greenland	1290	67.0^0N	50.95^0W	15+	3
EISCAT Svalbard Radar	500	78.1^0N	15.1^0E	20+	−1
Resolute Bay (Nunavit, Can.)**	450	75.0^0N	95.0^0E	100+	−6 h

*Decommissioned; **Under construction.

Along with the relationship between the kT and the transmitted wave and ks, the radar scatters over medium, km regulations. The first ion and electron simultaneously dispersion line findings (so-called lines of plasma).Data have been collected over Arecibo, which is the dominant ion, at altitudes 1460 to 2486 km [189] (Figure 2.7).

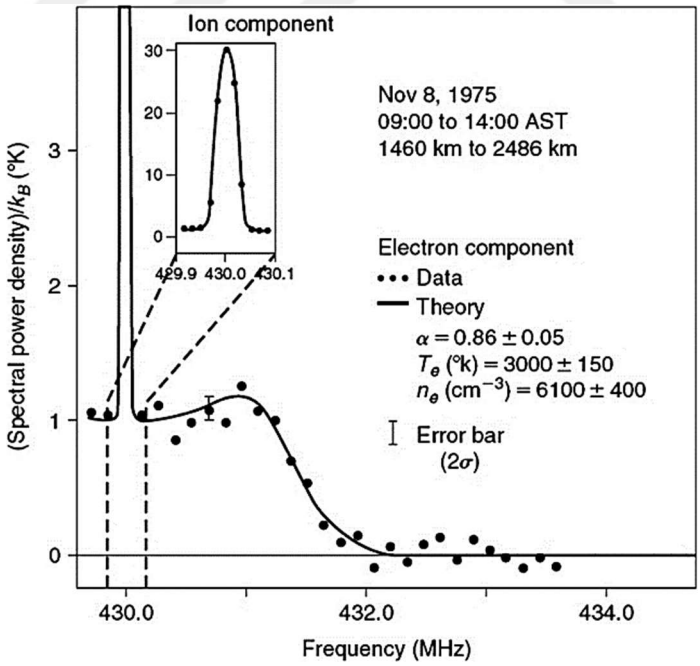

Figure 2.7. The first simultaneous ion and electron dispersion line findings (called plasma lines). Data were gathered over Arecibo, where H+ is the dominant ion, from 1460–2486 km in altitude [190].

As time varies about 200 km, the plasma and gyro lines. Last are magnetized magnetic plasma electrostatic waves that occur in the thermal balance of the electromagnetic branch in whistler-mode [172] (Figure 2.8).

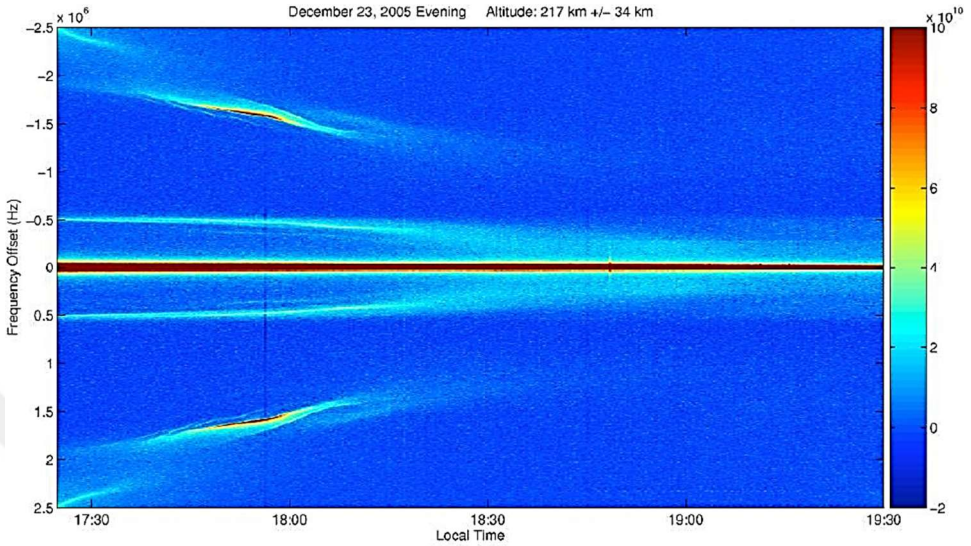

Figure 2.8. As a function of time around 200 km, the plasma and gyro lines [172].

2.10.2. Total Electron Content (TEC)

The ionosphere is a space in the altitude of between 50 and 1000 km with charged particles containing ions and electrons. The freely-electric ionosphere density is greatly assigned to some atmospheric parameters, to affect the propagation of electromagnetic radiofrequency waves. The primary causes for this instability Wind/magnetic wind and solar are even lower atmospheric processes. The global positioning system, which is used extensively for ionosphere analysis [173–174] and indicates a cumulative number of electrons per observer in the ionosphere, provides a significant ionosphere-spread parameter. The TEC Unit (TECU) are 10^{16} electrons/m^2. It is estimated. Two L-band frequency transmissions of GPS satellites (L_1=1575.42 MHz and L_2=1227.60 MHz) are all obtained from the 10.23(f_0) MHz fundamental frequency where $L_1=154f_0$ and $L_2=120f_0$. As these GPS signals cross the ionosphere, the carrier wave is progressing with a group delay (time delay that isdirectly proportionate to the TEC and inversely proportional to the frequency of the TEC), depending on the TEC, due to the dispersion of the ionosphere. The location accuracy of the GPS receiver is also decreased [175]. There have been some ionosphere simulations established over the last few decades to understand the physics, which influence the dynamic of the ionosphere. The models of the ionosphere are categorized into research, study and physical models. To set down an international standard to the definition of ionospheric parameters based on

scientific detection of ionospheric plasma by field or in-site calculation, the Ionosphere (IRI) project was launched Spatial ReferenceCommittee (COSPAR) and the International Radio Science Union (URSI) at the end of the 1960s. IRI describes mass, the temperature of the electron, ion temperature, ion structure. In addition, theelectron content at an altitude between 60 km and 2000 km at a given place, time and date. TEC isobtained from the IRI model using the computational integration of profiles for electron density (Ne-H). The models of IRI are constantly developed based on new information and modeling solutions IRI defines electron density, electron temperature, ion temperature, ion composition andthe electron contents at an altitude between 60 km and 2000 km at a given place, time and date. TEC is obtained from the IRI model using the computational integration of electron density (Ne-h)profiles. The new knowledge and modeling approach [176–178] has been used in the constant development of the IRI model. Bottom-side profiles below the F2-peak were compared to the onesof multiple [179] monogram and incoherently scattered radars for low and high periods of solar activity at lower latitudes were observed in IRI-90 and IRI-95, as was expected in TEC overestimation during a low solar activity using these IRI models. These discrepancies have been due to improper IRI model profile forms. The model's accuracy relies on accurate data being madeavailable in a particular area and period.

2.10.3. Earthquake

An earthquake is the shaking off the face of the Planet and is the result of the rapid release of energy into the earth's lithosphere and causes seismic waves. This is also known as a shake, tremor or trembling. Earthquakes can range from the vulnerable to the aggressive ones thatcan't sense them and catapult objects and people into the air and kill whole towns. The seismicity of a region is the magnitude, form and scale of the earthquakes that have occurred during a given time. The term shake is often used for seismic rumbling without an earthquake. Earthquakes occur on the earth's crust by stirring up and shifting or disturbing the earth. When the epicenter is underwater, the seabed will be displaced enough to trigger a tsunami. Earthquakes may also trigger earthquakes and volcanic activity periodically. The term earthquake, in its most general sense, is used to describe any natural or human- induced seismic phenomenon that causes seismic waves. The causes of earthquakes are mostly seismic fault breaking, but also other activities such as volcanic eruption, landslides, mine blasting,and nuclear testing. The immediate rupture of an earthquake is called its hypocenter. At ground level, the epicenter is right above the hypocenter [180].

2.10.4. Methods of prediction

The prediction of an earthquake is unacceptable technology — no earthquake from the first values had yet successfully forecast. Therefore, research into the prediction methodology is based

on empirically analyzed, two methods in general: to identify distinct earthquake precursors or to identify some sort of geophysical seismic trend or pattern that may lead to a major seismic seizure [181]. Precursor methods are mostly chosen because of their possible use for predicting or predicting short-term earthquakes, whereas predictive, long-term (10-100-year time scale), and intermediate-term (1-10-year time scale) methods for forecasting are normally considered useful [182].

2.10.5. Precursors

A seismic precursor is an exception in which an imminent earthquake may be effectively alerted [183] these reports – although commonly known as such only after the case – the amount in thousands [184], some of which date from ancient times. In the scientific literature, some 400 records of potential precursors, ranging from agronomy to zoology, have been made [185-186], ofapproximately 20 forms [187] none of the earthquake forecasts has been considered accurate [188].

The IASPEI called for the Provisional list of important precursor nominees at the beginning of 1990. There were 40 nominations, five of which were chosen to be major precursors, two based on one finding [189]. The ICEF was finalized in 2011 after a critical review of scientific literature that "considerable space for methodological changes in such research is available" [190]. Many instances of recorded precursors are, in fact, inconsistent, lack amplitude measurements or are not necessarily appropriate for a detailed statistical assessment. The findings released are favorable and False Negative Rate (earthquake but no precursory) [191].

2.10.6. Emission of radon

Most rocks absorb a small number of gases that can be distinguished from normal atmospheric gasses. Spikes in the concentration of these gasses are recorded before a major earthquake; this is because of pre-seismic or rock fracture. All of these gasses are Rn, which is caused by the radioactive decay of uranium in much of the soil [191]. As a possible Earthquake Predicted, radon is valuable because it is unstable and hence can be readily detected [192] its brief half-life (3,8 days). In the 2009 study [193] 125 records of improvements in radon levels have been identified since 1966 before 86 earthquakes. However, as the ICEF noticed in its analysis, up to one thousand kilometers, months later, on all sizes the earthquakes that were allegedly connected with those shifts. Anomalies were found in some cases in faraway places, but not nearer places. "No important relationship," the ICEF found [194].

2.10.7. Electromagnetic Anomalies

Electromagnetic disruption findings The Great Lisbon 1755 earthquake, but almost all such finds have been since the middle of the 60's and their attribution to the earthquake fails process were unfounded because the methods used had a sensitivity to physical motion [195]. Several anomalous electric, electrical-resistant and magnetic effects have since been linked to the preceding stress and strain shifts [196], which have led to expectations that a stable earthquake counterpart would be found [197]. While a handful of researchers are attentive both to hypotheses on how these phenomena can be produced, reports that these phenomena have been detected before no earthquake has been a true precursor. An analysis of the ICEF 2011 discovered that Magnetic anomalies with the low frequency were "most persuasive," according to the International Commission for Earthquakes for Civil Protection (ICEF) [191]. However, discovery is now believed to be a flaw of the method. A closelyfollowed research in 2004 further analysis indicates the lack of large transient signals from earthquakes under five. However, that there were no signs of any kind of precursory electromagnetic signal [198]. The ICEF found that it had failed to find useful precursors [191].

2.10.8. Spread of Dilatancy

In the seventies, the theory of the Spread of Dilatancy was widely respected as a foundation for different processes perceived to be potential precursors to earthquakes [199]. It was based on "strong and recurring evidence" [199] from lab tests that showed a change in size or dilatancy of highly stressed crystalline rock [200]. This leads to change other functions, including seismic speed, electric resistivity, and on a wide scale topographical uplift. This was assumed to be done only before the earthquake in a "preparatory stage," and so adequate control could alert against a forthcoming earthquake [201-202]. Numerous reports have nevertheless doubted the results [203] and consequently languishedthe theory. The retrospective collection of parameters was another factor [199, 204]. Otherexperiments have found the dilatancy of a large-scale prepared zone, which indicates that the occurrence is expected to come, to be so small that it persists as the ether was not contained in theexperiment Michelson-Morley. Friedman Freund discovered in his research on crystalline physics those molecules of waterintegrated into rock are under heavy stress, it can dissociate into ions. Under certain conditions, thecarriers that result will produce currents in the battery. Freund proposed that the earthquake precursors such as electric waves, earthquake lights and ionosphere disorders may have these currents. The observation of these currents and interactions is called Friendly Physics [205–207]. Most seismologists oppose Freund's suggestion that for various reasons, signals produced by stress can be identified and used as precursors. First, tension does not accumulate immediately until a serious earthquake and so it is unlikely that broad

currents can quickly form. Second, seismologistshave thoroughly searched and used sophisticated instruments for statistically accurate electric precursors, and no such precursors have been found. Thirdly, water in the crust of the earth will absorb any formed streams to the surface [206].

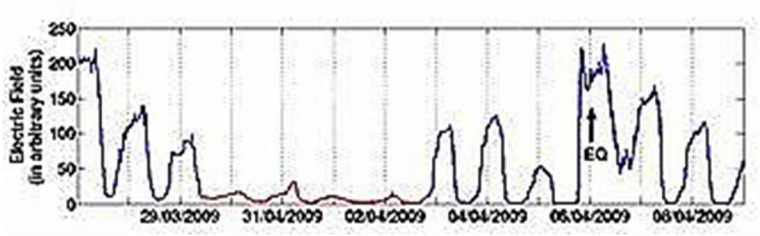

Figure 2.9. The reported ULF* of the ionosphere retention D layer that absorbs EM radiation [206].

The lower D-layer of the ionosphere by day while the plasma becomes gas in the night. At night, in higher altitudes than at layer D (Figure 2.9), the ionosphere's F-layer stays established. During the night(sky wave spreading) a waveguide is created Radio frequencies when the F-layer is shown on the waves to the ground for low HF up to 10 MHz. During the day, the heaven wave is lost when thosewaves are being collected by layer D (Figure 2.10). It is said that the tectonic tension The waves of electric charge in the earth's crust [208] travelto the Earth's surface to impact the ionosphere [209]. ULF* regular ionosphere ion cycle records show that a few days before a shallow severe earthquake a common cycle could be disrupted (Figure 2.10). When a disorder happens, either a D-layer is lost throughout the day, increasing theionosphere and a development of sky waves. At night, the D-layer becomes smaller in the ionosphere [210–211]. A network of VLF transmitters and receivers is installed at research centers globally to monitor shifts in sky waves. Each receiver often operates inside the network at a daisy transmissionfor distances of 1000-10,000 kilometers. Based on the network density, the general area under excitation will be calculated [212–213]. In the other hand, it was seen that globally extreme ones, such as magnetic or solar flares and local extremes, existed in the foreseeable future when the sitewas measured in the same VLF direction as another earthquake or volcanic eruption. Has it found the connection with the earthquake of interest difficult or impossible to change the sky wave? [214].

3. MATERIAL AND METHODS

This section would address the field of research property and location, meteorological data and characteristics, TEC, geomagnetic activity, and methods for surveillance on the soil by using ARIMA and MCS.

3.1. Autoregressive Integrated Moving Average (ARIMA)

The ARIMA model is a generalization of the ARMA model in statistics and econometrics, especially in time serial analysis. This is the model of the autoregressive integrated moving average. Both models may be used to view the data in time series or estimate future series points (forecasting). In certain cases, where the data show non-stationary effects, ARIMA models are applicable, but not variance/auto covariance (Note: ARIMA models) and when one or more times (equivalent to the "integrated" component of the model) the initial differential step may be inserted (i.e., the trend) [215]. The seasonal differentiation [216] may be used in the exclusion of the seasonal aspect where the seasonality is seen in a time sequence. As the ARMA model is logically adequate to represent a large-scale fixed time series, according to the decomposition theorem of Would, [217–218] it is reasonable, for example using differentiation, to make a non-stationary time series stationary, to be included in the ARMA model [219]. The MA part shows the regression error is a linear combination of error words, the values ofwhich were presented in the past at different times [220] means that the data value was replaced bythe discrepancy between its values and the values previously indicated by I (for "integrated") (and more than once, this mechanism of differentiation has been conducted). Both of these features are developed to make the model as suitable as possible for results. The ARIMA model is usually denoted in non-seasonal models ARIMA (p,d,q) with parameters p, d, and q as non-negative integrals, p as the auto-responsive model (number of time lags), d as the difference between the parameters (the number of times past data values have been subtracted), Q as the moving-average model. ARIMA (p,d,q)(P, D, Q)m, in which m corresponds to the number of cycles for each season, and the auto regression, differentiation and average movement terminology for the seasonal portion of ARIMA are referred to as the uppercase P, D, Q [216, 221].

The model could be referenced by removing the acronym defining the model with the non-zero parameter "AR," "I" or "MA." It is AR (1), I(1), and MA, for example (1). ARIMA is the most widely used predictive tool. The model is written as ARIMA (p, d, q) inwhich p is the order in which the car regressive mechanism is performed, d is in the order of data, and q in the order of movements [222-223]:

(a) Model identification; only stationary time series data can be used for the ARIMA model. This is why the first step is to analyze whether or not the time series data are stationary.

(b) Parameter identification (ACF and PACF); the value of d (stationary data) and the amount of residual lag (q) and the dependent lag value (p) used for the model must be calculated to use the ARIMA model. ACF and PACF (Partial Auto Correlation Function) are the key methods used to classify q and p and the correlation that displays the graph of ACF or PACF for lags. The partial coefficient of self-correlation tests the level of closeness between X_t and X_{t-k} and is considered consistent in the laboratory effect periods 1, 2, 3,…, k-1.

(c) Choice of the best variant of ARIMA; Some alternative models of ARIMA will be generated from the results of the stationary recognition and identification of ACF and PACF. Estimate the regressive auto parameters hereafter.

(d) Forecasting; The future cycle can be predicted until the best model has been achieved. In certain cases, this approach is more accurate to predict than to predict by other time series methods [224]. The average observations for a certain time series are E [wt] = wt, the medium estimator, written,

$$\varpi_t = \frac{1}{t}\sum_{t-1}^{\tau} \omega_t \tag{3.1}$$

3.1.1. Autocorrelation Function (ACF)

The covariance between a permanent phase ω_t and $\omega_t + k$ is

written as $\gamma k = Cov(\omega_t, \omega_{t+k}) = E[(\omega_t - \mu)(\omega_{t+k} - \mu)]$ (3.2)

and the connection between ω_t and $\omega_t + k$ as

$$\rho_k = \frac{Cov(\omega_t, \omega_{t+k})}{\sqrt{Var(\omega_t)}\sqrt{Var(\omega_{t+k})}} = \frac{\gamma_k}{\gamma_0} \tag{3.3}$$

where Var (ω_t) is 0 [225].

3.1.2. Role of partial autocorrelation (PACF)

The Partial autocorrelation function is helpful for the order of the self-reaction mechanism provided by the Yule-Walker equations,

$$\rho_1 = \varphi_{k1}\rho_0 + \varphi_{k2}\rho_1 + \cdots + \varphi_{kk}\rho_{k-1}$$

$$\rho_2 = \varphi_{k1}\rho_1 + \varphi_{k2}\rho_0 + \cdots + \varphi_{kk}\rho_{k-2} \tag{3.4}$$

$$\vdots \qquad\qquad \vdots$$

$$\rho_k = \varphi_{k1}\rho_{k-1} + \varphi_{k2}\rho_{k-2} + \cdots + \varphi_{kk}\rho_0$$

The Yule-Walker equations are marked with R = A.P in the matrix form, while

$$R = \begin{bmatrix} \rho_1 \\ \rho_2 \\ \vdots \\ \rho_k \end{bmatrix}, \quad A = \begin{bmatrix} \rho_1 & \rho_1 & \cdots & \rho_{k-1} \\ \rho_2 & \rho_2 & \cdots & \rho_{k-2} \\ \vdots & \vdots & \ddots & \vdots \\ \rho_k & \rho_k & \cdots & \rho_0 \end{bmatrix}, \text{ and } \quad P = \begin{bmatrix} \varphi_{k1} \\ \varphi_{k1} \\ \vdots \\ \varphi_{kk} \end{bmatrix}. \tag{3.5}$$

The assessment is φ_{kk} Using Cramer's law to get. In other terms,

$$\varphi_{11} = \rho_1, \ \varphi_{22} \quad \begin{bmatrix} 1 & \rho_1 \\ \rho_1 & \rho_2 \\ \hline 1 & \rho_1 \\ \rho_1 & 1 \end{bmatrix}, \quad \varphi_{33} = \begin{bmatrix} 1 & \rho_1 & \rho_1 \\ \rho_1 & 1 & \rho_2 \\ \rho_2 & \rho_1 & \rho_3 \\ \hline 1 & \rho_1 & \rho_2 \\ \rho_1 & 1 & \rho_1 \\ \rho_2 & \rho_1 & 1 \end{bmatrix}, \tag{3.6}$$

and so on.

3.1.3. Time Series Models Stationary

Stationary time series models, which are constant in mean, are derived from non-trending series. In the following pages, the family of self-adjustment models is discussed.

Process of Auto regression (AR) The autoregressive general order is determined by

$$\omega_t = \varphi_0 + \varphi_1 + \omega_{t-1} + \varphi_2 + \omega_{t-2} + \cdots + \varphi_p + \omega_{t-p} + \varepsilon_t, \tag{3.7}$$

where "t is a medium-zero, white noise process variance. The $\varphi_1, \varphi_2 \cdots, \varphi_p$ are self-representing model parameters, is ε_t Constant findings and ω_t are a φ_0 stationary time series. From (Eq 3.7), the is given by

$$\varepsilon_t = -\varphi_0 - \varphi_1 + \omega_{t-1} - \varphi_2\omega_{t-2} - \cdots + \varphi_p\omega_{t-p} +, \omega_t,$$

It follows that with backshift operator B

$$\begin{aligned}\omega_t - \mu &= \varepsilon_t - \vartheta_1\varepsilon_{t-1} - \vartheta_2\varepsilon_{t-2} - \cdots - \vartheta_q\varepsilon_{t-q} \\ &= (1 - \vartheta_1 B - \vartheta_2 B^2 - \cdots - \vartheta_q B^q)\varepsilon_t \\ &= \vartheta_q(B)\varepsilon_t.\end{aligned} \tag{3.8}$$

Equation (3.8) is a back-shifting AR(p) construct. Process Move Average (MA) The general order of the average moving phase is indicated by

$$\omega_t = \mu + \varepsilon_t - \vartheta_1\varepsilon_{t-1} - \vartheta_2\varepsilon_{t-2} - \cdots \vartheta_q\varepsilon_{t-q} \tag{3.9}$$

where "t's a medium zero white noise phase σ^2 and variance. The $\vartheta_1, \vartheta_2, \cdots \vartheta_q$ are moving average parameters, is the mean, and ω_t are data points that depend on time, and are stationary. From (15) the backshift operator moving average is written as,

$$\begin{aligned}\omega_t - \mu &= \varepsilon_t - \vartheta_1\varepsilon_{t-1} - \vartheta_2\varepsilon_{t-2} - \cdots \vartheta_q\varepsilon_{t-q} \\ &= (1 - \vartheta_1 B - \vartheta_1 B^2 - \cdots \vartheta_q B^q)\varepsilon_t \\ &= \vartheta_q(B)\varepsilon_t.\end{aligned} \tag{3.10}$$

Average moving self-regressive (ARMA) The mixed p^{th} and q^{th} order model for the autoregressive mobile average model is [225-227],

$$\begin{aligned}&\omega_t - \varphi_1\omega_{t-1} - \varphi_2\omega_{t-2} - \cdots - \varphi_p\omega_{t-p} = \varepsilon_t - \vartheta_1\varepsilon_{t-1} - \vartheta_2\varepsilon_{t-2} - \cdots - \vartheta_q\varepsilon_{t-q}, \\ &\omega_t - \varphi_1 B\omega_t - \varphi_2 B^2\omega_t - \cdots - \varphi_p B^p\omega_t = \varepsilon_t - \vartheta_1 B\varepsilon_t - \vartheta_2 B^2\varepsilon_t - \cdots - \vartheta_q B^q\varepsilon_t\end{aligned} \tag{3.11}$$

$\varepsilon_t \sim (0, \sigma^2)$ Where WN. - Where WN. This model's parameters are $\varphi_1, \varphi_2, \cdots, \varphi_p$ and $\vartheta_1, \vartheta_2, \cdots, \vartheta_q$ The application to the above equation of the back shift operator,

$$\begin{aligned}&\omega_t - \varphi_1 B\omega_t - \varphi_2 B^2\omega_t - \cdots - \varphi_p B^p\omega_t = \varepsilon_t - \vartheta_1 B\varepsilon_t - \vartheta_2 B^2\varepsilon_t - \cdots - \vartheta_q B^q\varepsilon_t \\ &(1 - \varphi_1 B - \varphi_2 B^2 - \cdots - \varphi_p B^p)\omega_t \quad = (1 - \vartheta_1 B - \vartheta_2 B^2 - \cdots - \vartheta_q B^q)\varepsilon_t \\ &\qquad\qquad \varphi_p(B)\omega_t = \vartheta_q(B)\varepsilon_t\end{aligned} \tag{3.12}$$

where $\varphi_p(B) = ((1 - \varphi_1 B - \varphi_2 B^2 - \cdots - \varphi_p B^p)$, and

$\vartheta_q(B) = (1 - \vartheta_1 B - \vartheta_2 B^2 - \cdots - \vartheta_q B^q)$

3.1.4. Akaike's Information Criterion (AIC)

The AIC is defined [225],

$$\mathrm{AIC}(N) = \tau \ln \hat{\sigma}_{\varepsilon}^{2} + 2N \tag{3.13}$$

where N is the number of parameters in the model, is τ the number of observations, and

$$\hat{\sigma}_{\varepsilon}^{2} \frac{\sum_{t=p+1}^{\tau} \varepsilon_t^2}{\tau - (2p + q + 1)}, \tag{3.14}$$

$\varepsilon_t = \omega_t - \hat{\omega}_t, \hat{\omega}_t$ Where the model values are estimated, and p and q are pattern instructions.

3.1.5. Testing portmanteau Ljung-Box

Also, a portman's courtroom is the Ljung-Box. This is a clone of Box-Pierce that has been updated. Simulation experiments showed that Ljung-Box testing is best for all sample dimensions, including small samples [228].

$$Q = \tau(\tau + 2) \sum_{k=1}^{h} \frac{\rho_k^2(\hat{\varepsilon})}{\tau - k}, \tag{3.15}$$

where $\tau = T - d.$ The crucial area is the same as the Box-Pierce test.

3.1.6. Forecasting

For the prediction of potential prices, the forecasting is used. The consistency and quantitative prediction are two methods of prediction. Qualitative projections are mostly used where there are no statistics available and are based on experts' observations and opinions. Quarantine forecasts are on the other hand a tool which estimates future values on the basis of past observations. This approach also allows the data to be accessible.

Example: The expected equation is given for an IMA(1,1).

$$\hat{z}_t = \varepsilon_t - \vartheta_1 \varepsilon_{t-1}, \tag{3.16}$$

$\hat{z}_t = \nabla \hat{w}_t$ Where now suppose that $\hat{\vartheta} = 0.65$ is

$$\hat{z}_t \_ 0.65\varepsilon_{t-1}, \quad \varepsilon_t \sim WN(0,\sigma^2). \tag{3.17}$$

The predicted values can be derived from this equation. The predicted values for nondifference observations, ω_t, are calculated in non-deference form, i.e. the rewriting equation (3.17)

$$w_t - w_{t-1} = -0.65\varepsilon_{t-1}$$
$$\hat{w}_t - w_{t-1} = -0.65\varepsilon_{t-1}.$$

Thus if the real t = 3 value is $\omega_3 = 579$ and the error is 16:01. The prediction value will then be for $\omega_4 = 576$,

$$\hat{w}_4 = 579 - 0.65$$
$$= 568.59.$$

For the same phase t = t + 1, and so on [229].

3.1.7. Role of partial autocorrelation (PACF)

The Partial autocorrelation function is helpful for the order of the self-reaction mechanism provided by the Yule-Walker equations,

3.2. Monte Carlo Method

Monte Carlo (MC) methods are a broad variety of calculation algorithms based on random repeated numerical samples. The basic principle is to use randomness to solve problems that may be deterministic in theory. Sometimes used in physical or quantitative problems, such approaches are more useful whether they are difficult or impracticable. MC methods are mainly used in three types of problems: optimization [230], numerical integration, and probability distribution. Monte Carlo methods for simulating various free systematics, such as fluids, disturbing components, closely bound solids, and cellular structures are useful for physics-related problems (see the model of Potts cellular, particle interacting systems, McKean-Vlasov processes, kinetic gasmodels) [231].

The principle can be used to solve a probabilistic study of all queries using Monte Carlo techniques. The integrals described by the expected random variable value are approximated by the large numbers law by the empirical average of the independent variable specimens (including samples). When the variable's probability distribution is parametrized, mathematicians also use a Monte Carlo (MCMC) Markov chain sampler [232–234]. The core concept is designing an intelligent Chain model for Markov with the fixed distribution of probabilities. Samples from the

ideal distribution (target) in other words are the samples that will be generated by the MCMC process [235–236]. The stationary distribution by the ergodic theorem, is approximated by analytical measurements of the MCMC sampler random states. In Most cases, the goal is to generate probability distributions that satisfy a non-linear equation of growth. These probability-distribution fluctuations can often be viewed as the distribution of Markov's random states whose odds depend on existing random status distributions[237–238]. In other examples, we have an increasingly complicated probability distribution flow Boltzmann–Gibbs is compliant with falling temperature and many others (Path Space Models withan extended time horizon). These models can also be seen as evolving the law of random Markov chain states [238, 239–254].

3.3. Study Area

One of the main areas for the slip of continents that form the neo-tectonic evolution of Turkey and the East Mediterranean region is the North Anatolian Fault zone (NAFZ, see Fig. 3.1). The seismic activity of the region is heavy and poses a high risk of heavily populated areas. Although the deep structure of NAFZ remains largely riddled with its significance for the overall understanding of massive strike-slip failure mechanism, Eurasian tectonics and earthquake period modeling. Detailed tomographic models in the Anatolian area that provide both the crust and the upper mantle with a clear 3D image are the cornerstone for further development. NAFZ, with the North Anatolian Fault (NAF), is situated within 1500 km of the triple junction Karliova in eastern Anatolia to the Marmara Sea. It began taking the form of a broad shear zone 11–5 Ma as a reaction to the Eurasian and Arabian plateau's north-south convergence and subsequent southwest extrusion of the Anatolian block [255]. Starting at 12 Ma ago, the strain location spread westward, creating a small fault area that entered the Marmara Sea only 200 Ka ago, on the eastern part of the shear zone. The fault zone today grows from a divide of 10 kilometers east to a division of 100 kilometers west [255]. The NAFZ is situated in the vicinity of the Izmir-Ankara and Erzincan sutures for most of its length (Fig. 3.1). The two sutures originated from Africa and Eurasia after the closing of the Neotethyan Ocean 60–15 Ma [257]. This indicates that the near-face expression of NAFZ is closely related to the lower, yet to be studied lithosphere zones of vulnerability. A strikingly frequent movement from east to west of large NAF earthquakes over many decades was already recognized in 1944 [258] and later successfully modeled by stress propagation [259] (Stein et al., 1997). The evolution of the shear zone and earthquake migration can be conducted more precisely when accurate knowledge is available about the lithospheric structure [260]. Which illustrates the need for the deeply resolved crust and top mantle tomographic models. Anatolia has been the focus of many recent tomography studies owing to its high seismic vulnerability and significance for Eurasian neotectonics (Figure 3.1). Although the crustacean structure was imaged by local Earthquake Tomography [261], the upper-mounted models [262] receptor functions and refract

profiles [263]

Figure 3.1. Anatolia's neotectonic diagram, with major fault zones (black lines following [264]), Tethyan Ocean sutures (blue lines following [247] and the Holocene volcanos; (red diamonds, after [265]). The North Anatolian Fault Zone (NAFZ) has shattered lines of transparency (adapted from [256]). (The reader is linked to the online edition of this article as an interpretation of the color comparisons of this figure's legend.)

Inverting the crust or themantle would entail the hypothesis that objects in the tomographic model, in particular in a shallowdepth, will occur in one case [266-267]. Due to the difficulties of simulating and inverting broadband seismic wave fields in earth models with high 3D heterogeneities, no reliable model of both crust and top manto underneath Anatolia is yet available. We have created a complete waveform reversal,which combines tele-seismic and regional data, to overcome this difficulty. This helps one to constrain the crust and the upper mantle simultaneously so that we can shed light on the relationshipbetween deep lithosphere formation and low tectonic characteristics.

3.3.1. Geographical Location

In the north-central Anatolia, Turkey has situated the province of Corum (39°54′20″N, 34°04′28″E longitude). The province consists of 536 villages, which form 14 districts of 12820 km^2 of administrative area. The district of Kargı is 106 km north of the town of Corum (Figure 3.2) [268].

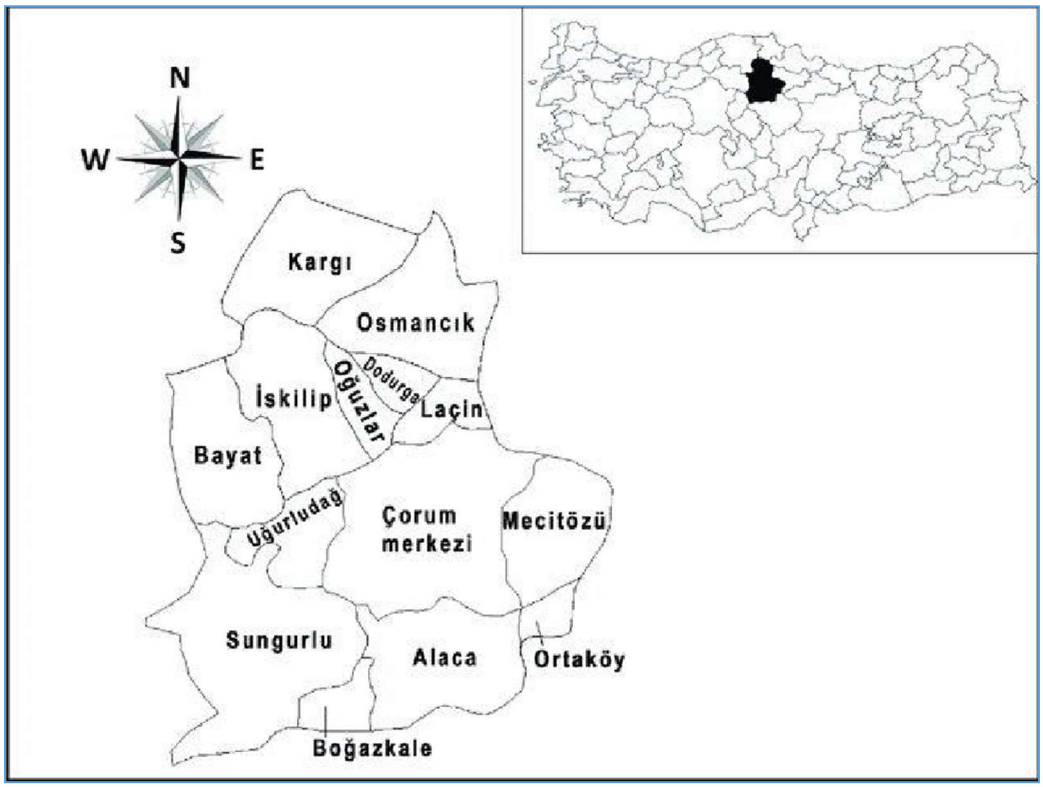

Figure 3.2. Map of the Corum province and its location within Turkey [269].

3.3.2. Climate

Çorum has a warm dry-summer continental climate with cold, cold summer and moderates to cool wet springs and light rain in the fall and springs (Köppen climate classification: dsb). The hottest times of Çorum province are in the months of July-August (≈ 29.0 ^{0}C), the average daily temperature in these months is ≈21 ^{0}C. The coldest days of the year are experienced in January (≈ −4 ^{0}C). Annual rainfall is an average of 444 mm per square meter. Monthly average sunbathing hours are 200 h [269].

4. RESULTS AND DISCUSSION

This chapter focuses on the statistical analysis of the ^{222}Rn soil concentration obtained in seismic stations in the Kargi area, the northern Anatolian Fault Zone (NAFZ), Turkey. This seismic position is seismically active. The field is listed as one of the most seismically active continental fault areas in the world. The influence of the earthquake thus substantially dominates the radon concentration. Other influences (temperature, humidity, pressure, etc.) such as meteorological variables may be considered non-predominant or regulated relative to the influence of earthquakes. During around 1 year, continuous or more accurately random records are called between Dec 16th, 2008, and December 31st, 2009 for 1,000 raw data of ^{222}Rn ground concentration from the soil at this site. Both data are considered within 15 min of brief measurement intervals. According to the time series review, ^{222}Rn levels are studied (Figure 4.1).

4.1. Applications of Monte Carlo and ARIMA

In this study, ARIMA and Monte Carlo simulations in accordance with the data were obtained after the time series analysis was performed considering the temporal changes of soil Rn gas samples. These simulations provide critical and statistically significant information for future Rn gas behavior.

4.1.2. Series Plot

Radon time series before implementing the ARIMA model is presented in Figure 4.1.

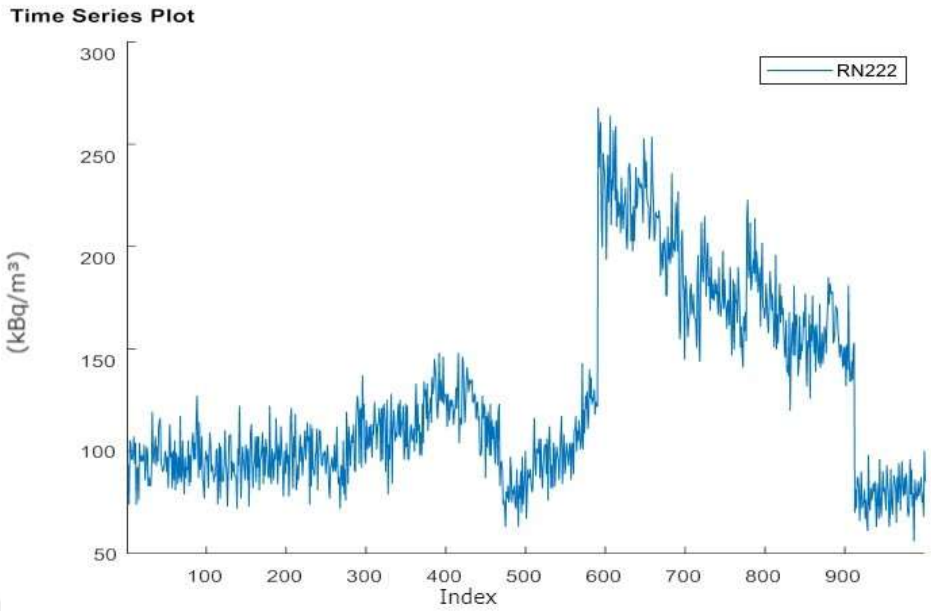

Figure 4.1. Time Series Plot of Rn-222

The differenced time series in order to achieve stationarity Rn-222 is the first-order difference in time series Rn-222 (Figure 4.2).

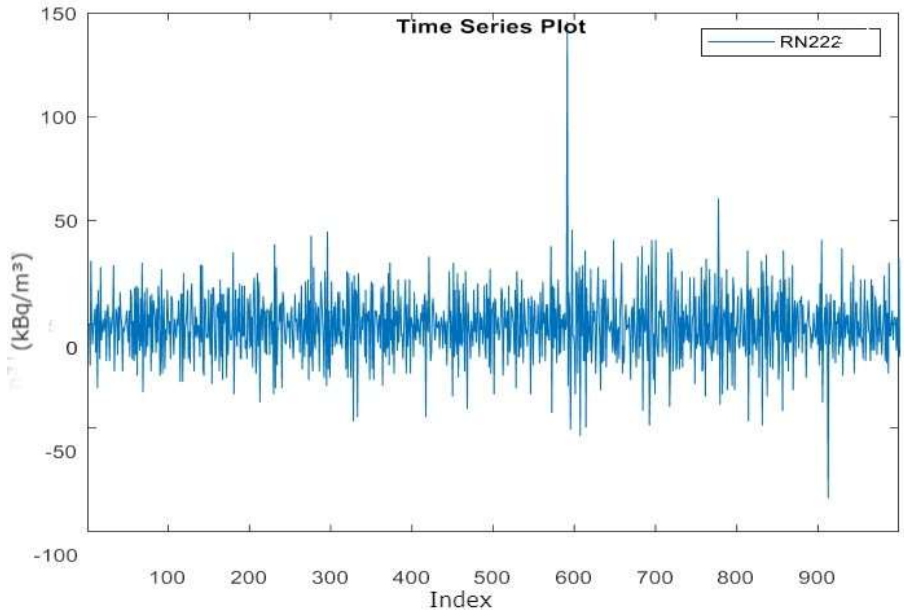

Figure 4.2. Time Series Plot of Rn-222 Diff

Augmented Dickey-Fuller Test

Null Hypothesis: Rn-222 Diff contains a unit root

$$y_t = c + \delta t + \phi y_{t-1} + \beta_1 \Delta y_{t-1} + \beta_p \Delta y_{t-p} + \varepsilon_t \quad (4.1)$$

$$H_a : \phi < 1$$

Before the ARIMA model was established, the Augmented Dickey-Fuller (ADF) test was performed to test whether advanced statistical analysis of the data could be performed. According to ADF test, Rn-222 Diff data include a one-unit branch (Eq.4.1). According to the test results 0.05 significance level (p-value = 0.001), the test statistic is -49.268 and the critical value is -1.942. Since the critical value is greater than the test statistics, it can be said that stability has been obtained. After applying dozens of ARIMA models to the data, the decision was made on the ARIMA (5,0,4) model (Table 4.3) with the smallest AIC and BIC values (Table 4.4) (AIC: 8152, 4417; BIC: 8206, 3507). Prediction parameters of the ARIMA (5,0,4) model are also given in Table 4.1 and Table 4.2. ARIMA (5,0,4) Model (Gaussian Distribution) (ARIMA Rn-222) of time series Rn-222 Diff with thefollowing equation:

$$(1 - \phi_1 L - \cdots - \phi_5 L^5) y_t = c + (1 + \theta_1 L - \cdots - \theta_4 L^4) \varepsilon_t \quad (4.2)$$

Table 4.1. Test Parameters

Lags	Model	Test Statistic	Significance Level
0	AR	t1	0.05

Table 4.2. Test Results

Null Rejected	P-Value	Test Statistic	Critical Value
true	0.001	-49.2685	-1.9416

4.2. ARIMA (5,0,4) Model (Gaussian Distribution) (ARIMA Rn-222)

After the time series analysis of the Rn data, we wanted to obtain the most suitable ARIMA model that describes the characteristics of the data. After trying many ARIMA models, it was decided that the most suitable model meeting the above requirements was ARIMA (5,0,4) (Table 4.3, 4.4). An autoregressive integrated moving average model of time series Rn-222 Diff with the following equation:

$$(1-\phi_1 L-\cdots-\phi_5 L^5)y_t = c+(1+\theta_1 L-\cdots-\theta_4 L^4)\varepsilon_t \quad (4.3)$$

4.3. Model Estimation

Table 4.3. Estimation Results

Parameter	Value	Standard Error	T-Statistic	P-Value
Constant	-0.01408	0.19173	-0.073438	0.94146
AR {1}	0.20483	0.31118	0.65823	0.51039
AR {2}	0.16103	0.24812	0.64899	0.51635
AR {3}	-0.63101	0.13871	-4.5492	5.3837e-06
AR {4}	0.042055	0.094979	0.44278	0.65792
AR {5}	0.047631	0.057372	0.83022	0.40641
MA {1}	-0.8452	0.31119	-2.7161	0.0066065
MA {2}	-0.098501	0.28191	-0.3494	0.72679
MA {3}	0.7476	0.23507	3.1803	0.0014711
MA {4}	-0.41345	0.12184	-3.3933	0.00069045
Variance	202.1185	3.8897	51.963	0

Table 4.4. Goodness of Fit

AIC	8152.4427
BIC	8206.3507

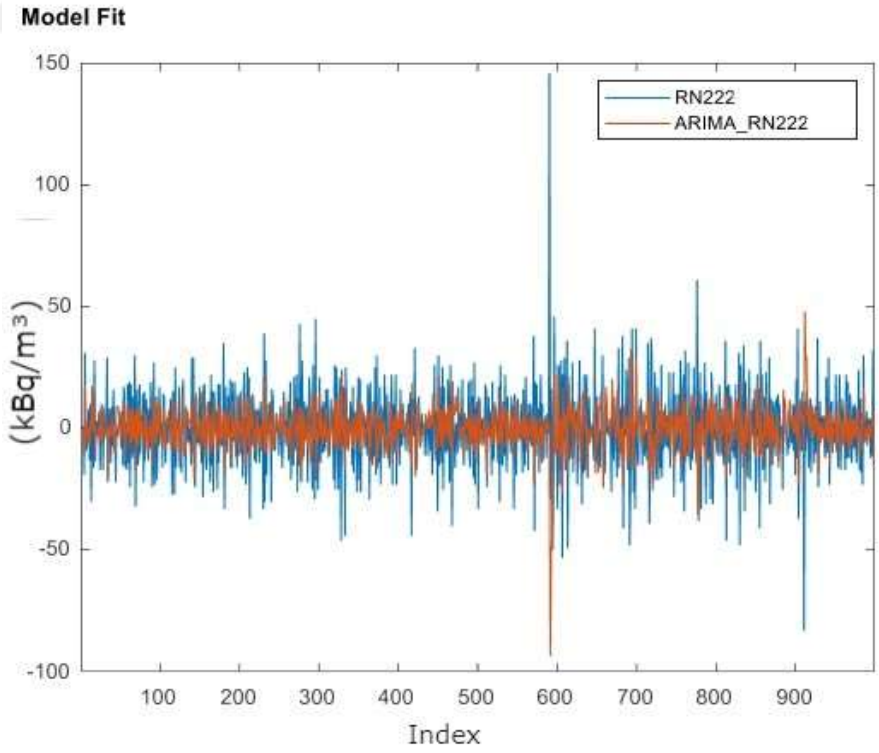

Figure 4.3. Plot the fit of the model ARIMA_Rn-222 time series

The residuals plot obtained from the ARIMA (5,0,4) model is given in Figure 4.3. The curve

of the model we obtained from ARIMA (5,0,4) and the curve we obtained from the first-order difference operation of Rn-222 can be seen in Figure 4.3. The histogram curve of the ARIMA (5,0,4) model data are given in Figure 4.4. Accordingly,it was seen that the data fit the normal distribution. This indicates that advanced statistical procedures can be performed.

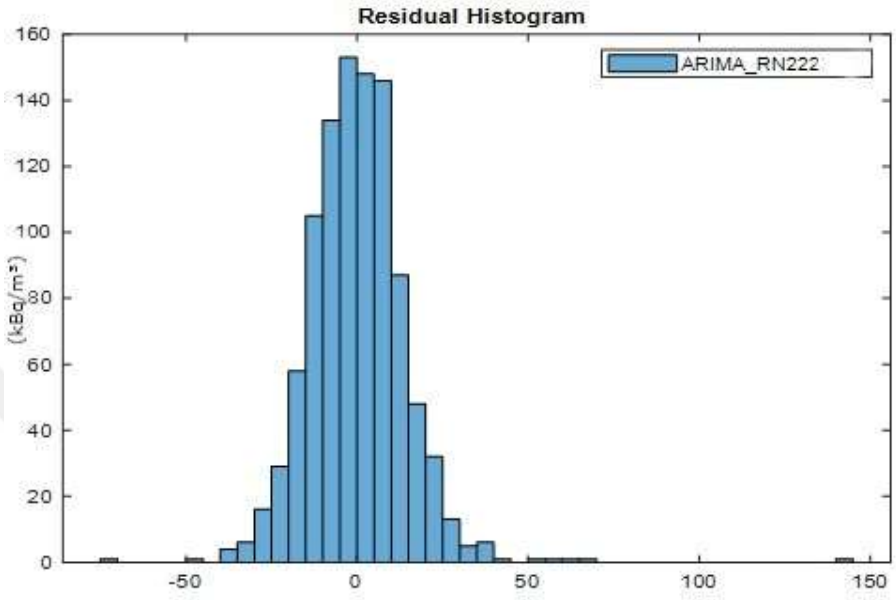

Figure 4.4. A histogram of the residuals of model ARIMA_Rn-222 .

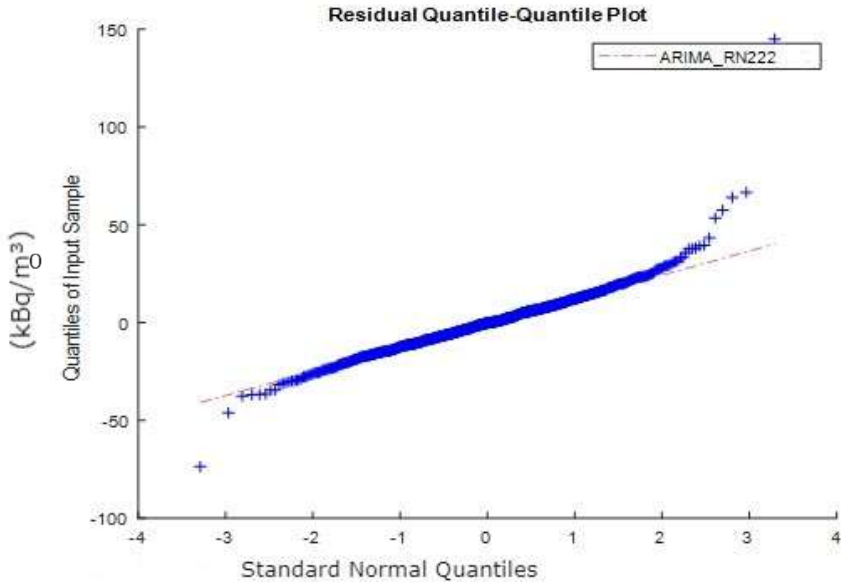

Figure 4.5. Quantile-quantile plot of the residuals of model ARIMA Rn-222 .

Q-Q plot graph, which can be another test method for the statistical compatibility of the

results obtained from the ARIMA Rn-222 procedure, is obtained in Figure 4.5. The sequence of changes on the ARIMA (5,0,4) model shown as the dashed line in Q-Q plot graphs is on a straight line. ACF graph obtained in Figure 4.6 can be seen. ACF can view the chart. The ACF chart shows that the data are stable.

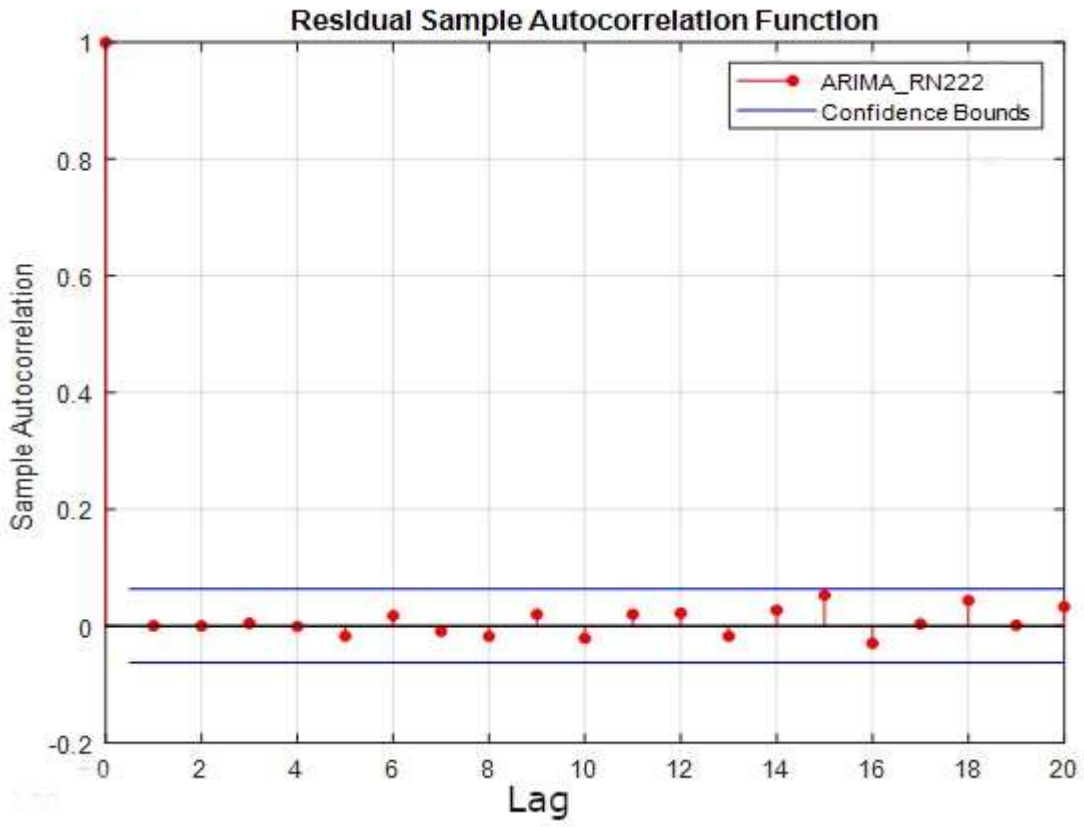

Figure 4.6. Sample autocorrelation function of the residuals of ARIMA_Rn-222

Ljung-Box Q test was performed to see auto-correlations of residual data. The parameters obtained for the test are as follows (Table 4.5 and Table 4.6). Null Hypothesis: The first m autocorrelations of the residuals of ARIMA Rn-222 Diff are jointly

$$H_0 : \rho_1 = \rho_2 = \cdots = \rho_m = 0$$
$$H_a : \rho_j \neq 0, j \in 1, \cdots, m$$

Table 4.5. Test Parameters

	Lags	DOF	Significance Level
1	20	20	0.05

Table 4.6. Test Results

Null Rejected	P-Value	Test Statistic	Critical Value
False	0.95583	10.6049	31.4104

4.4. ARIMA prediction of Rn-222 data

Figures 4.7 and 4.8 depict a Monte Carlo simulation of the model for 500 paths within 95% confidence bounds. The simulation curve seen is a mean simulation path for the 500 simulations. The Monte Carlo forecast was made for 100 paths from March 12th, 2009 and we have seen a rise in anomaly predicted by the Monte Carlo Forecast. The strength of this forecast will rely on the regression-fitting power that as seen was reasonable from the histogram and the Q-Q plot in Figures 4.4 and 4.5. Since the error is almost nearly normally distributed, we can say that the Monte Carlo forecast is to be plausible within the confidence bounds (Figure 4.7).

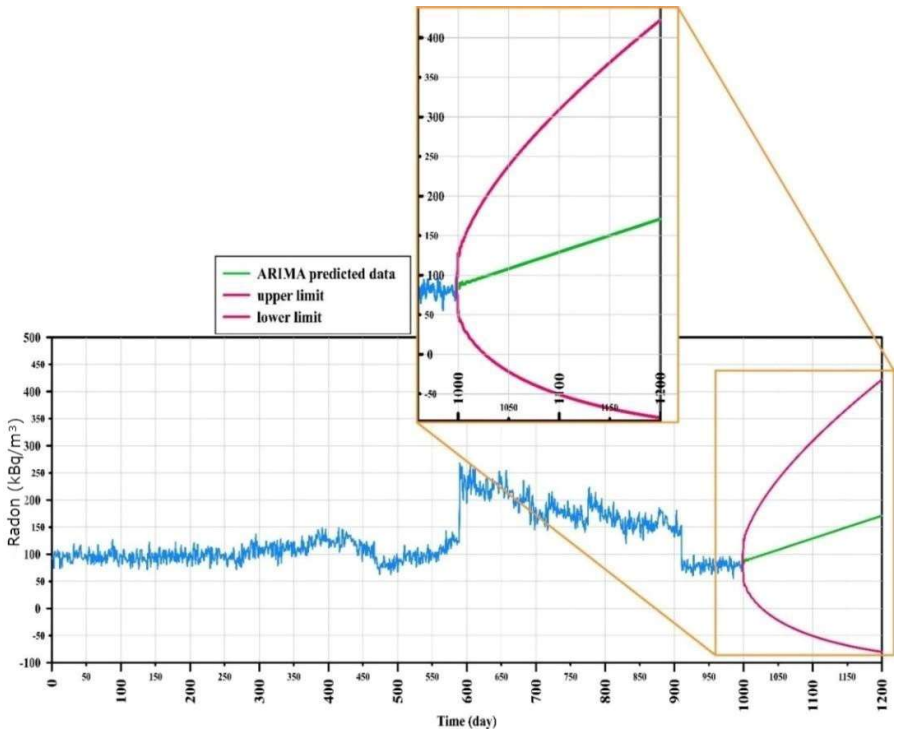

Figure 4.7. ARIMA prediction of soil Rn-222 data

4.5. Monte Carlo prediction simulation of Rn-222 data

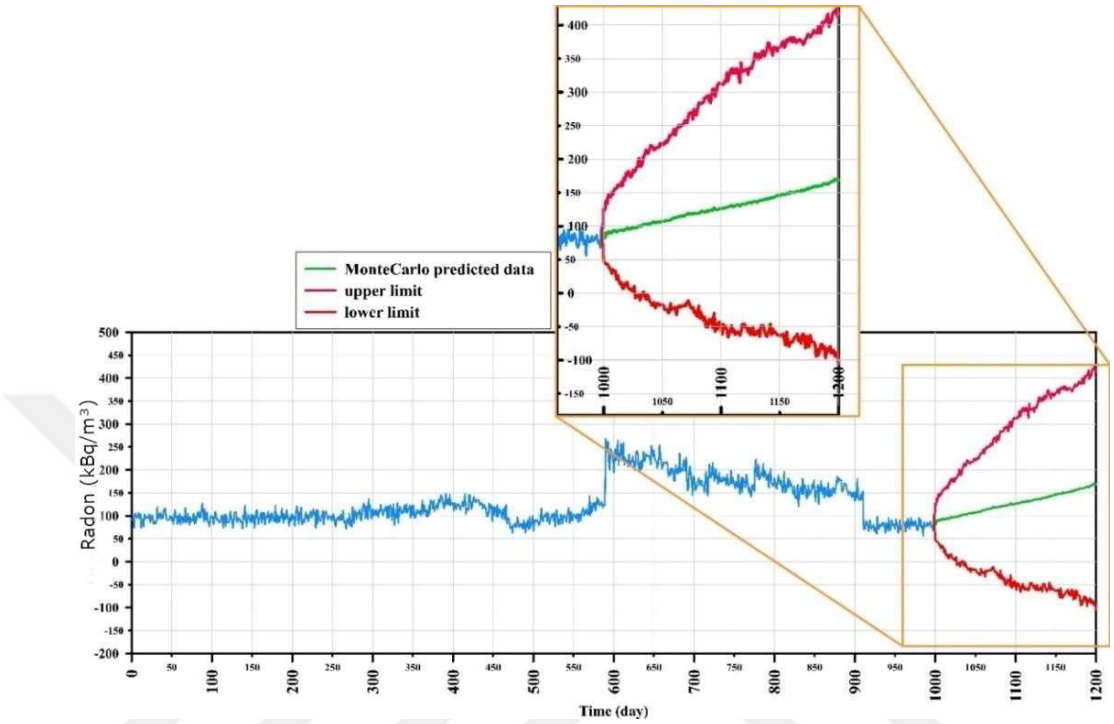

Figure 4.8. Monte Carlo prediction simulation of Rn-222 data

The results obtained were also successfully obtained in Monte Carlo simulations and are given in Figure 4.8. We saw that the model we suggested for the results of the data worked successfully. This situation will give significant strength to our further work.

4.6. Analysis of the Relation between Radon Gas, Soil temperate and TEC with Earthquakes

In this section, the earthquake data TEC and radon gas, in addition to the meteorological data, have been divided into three groups. Each group contains about 4 months of data, and the impact of earthquakes on these data will be discussed.

4.6.1. First Group

The first group starts on (Dec 16, 2008 to Mar 31, 2009), many micro-earthquakes occurred with magnitude (3 - 4.3), with TEC and radon concentration for the same period are shown in Figure 4.9.

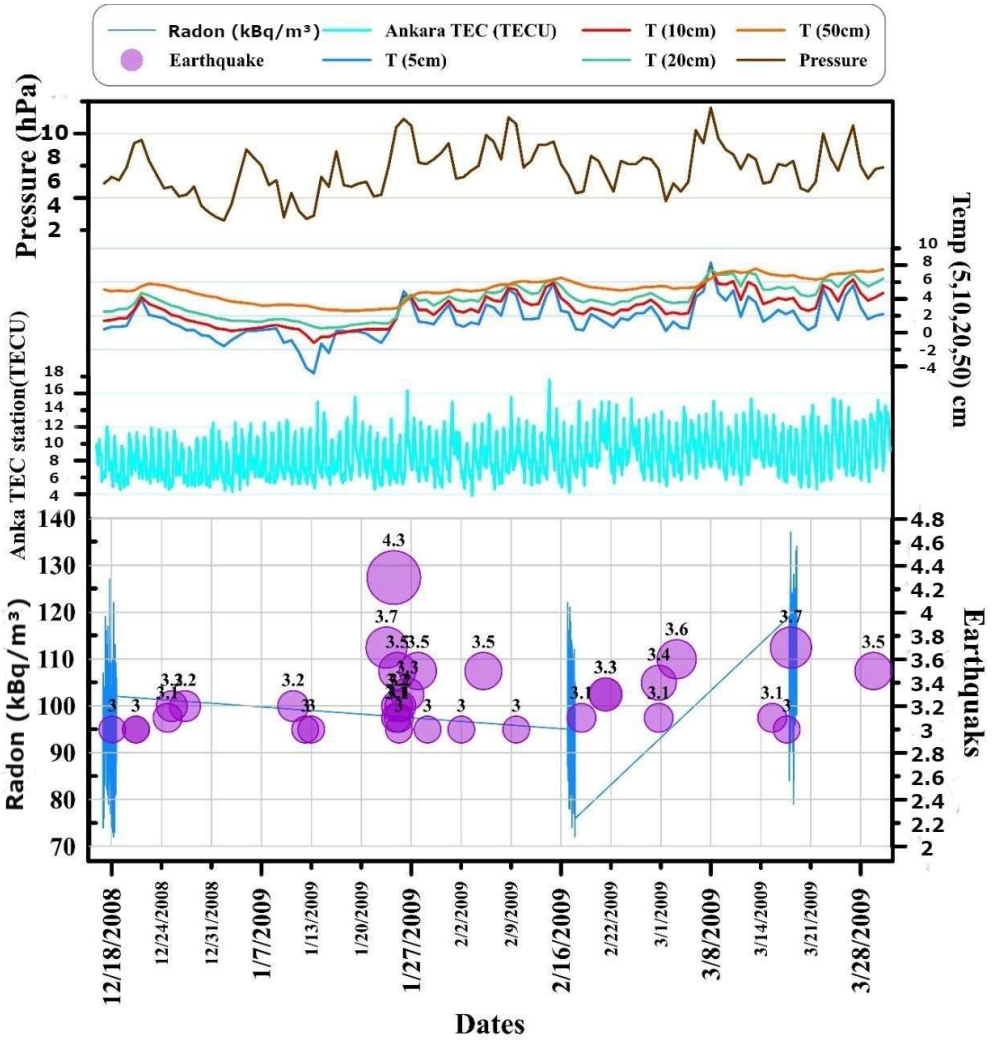

Figure 4.9. Radon, TEC, Temp of soil (5, 10, 20, and 50) cm and Pressure with Earthquakes for the Second group.

We can see that pressure is high and then slowly decrease from Figure 4.9. In addition, the second panel, we can see temperature be advertising diets. The temperature changes with the TEC, from trips we see the total electronic content decrease little before three points size of earthquake and they were a shape increase at the time of earthquake according it three-point to six. Also, we see Radon did not show any anomaly signal to render earthquake these details return to the geology of area.

4.6.2. Second Group

The third group starts on (Apr 1, 2009 to Aug 31, 2009), Many micro-earthquakes occurred with magnitude (3 - 4.4), with TEC and radon concentration for the same period are shown in Figure 4.10.

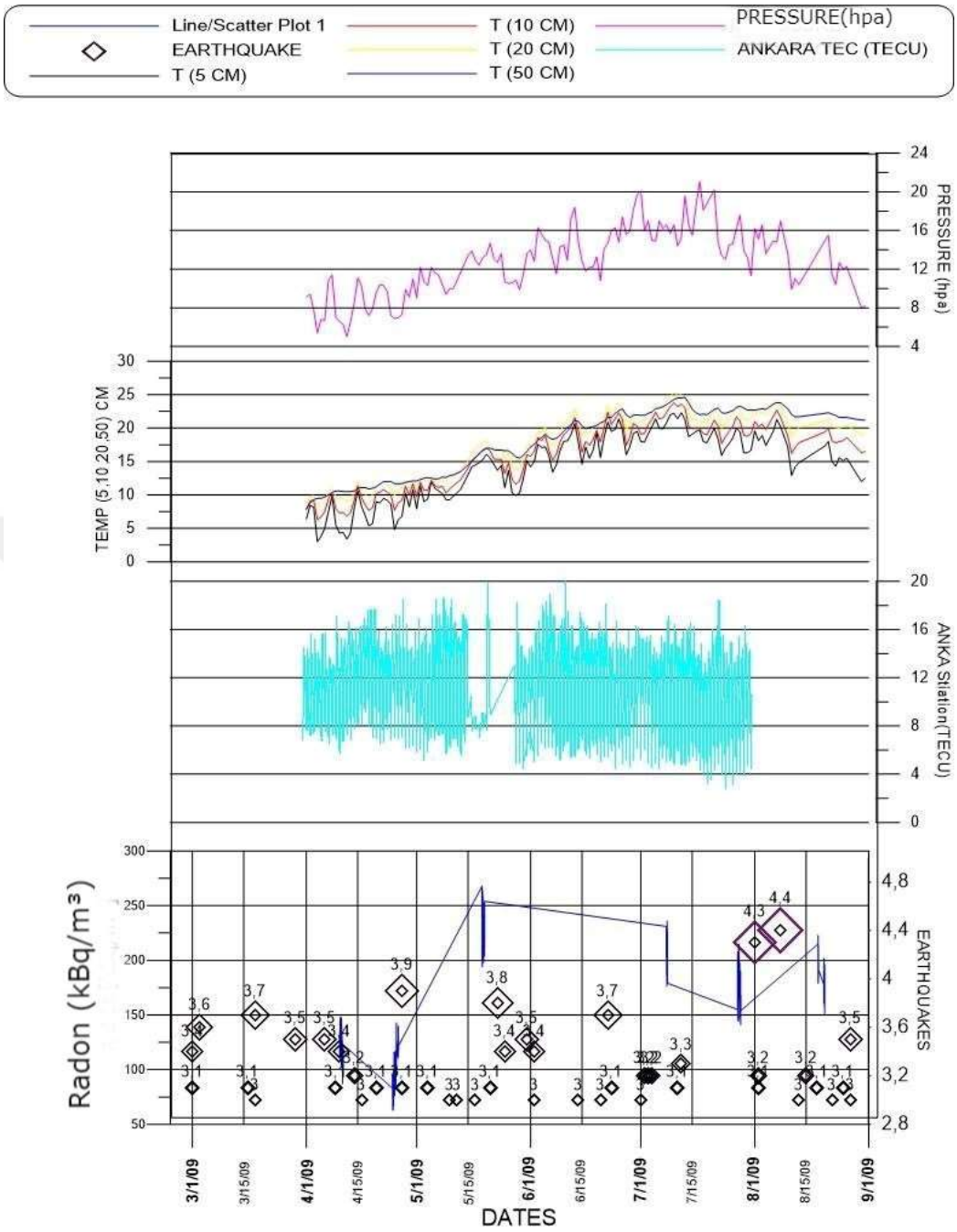

Figure 4.10. Radon, TEC, Temp of soil (5, 10, 20, and 50) cm and pressure with Earthquakes for the second group.

We see from the top panel that the pressure has risen slowly until it reaches too big then it decreases. In the lower panel, we see that the soil temperature decreases with TEC with increase TEC and increasing with increase TEC. The temperature at 5 cm is lower than the temperature at 10 cm also we notice that Radon spikes according to the earthquake.

4.6.3. Third Group

The third group starts on (Sep 1, 2009 to Dec 31, 2009), 11 micro-earthquakes occurred with magnitude (3 – 3.6), with TEC and radon concentration for the same period are shown in Figure 4.11.

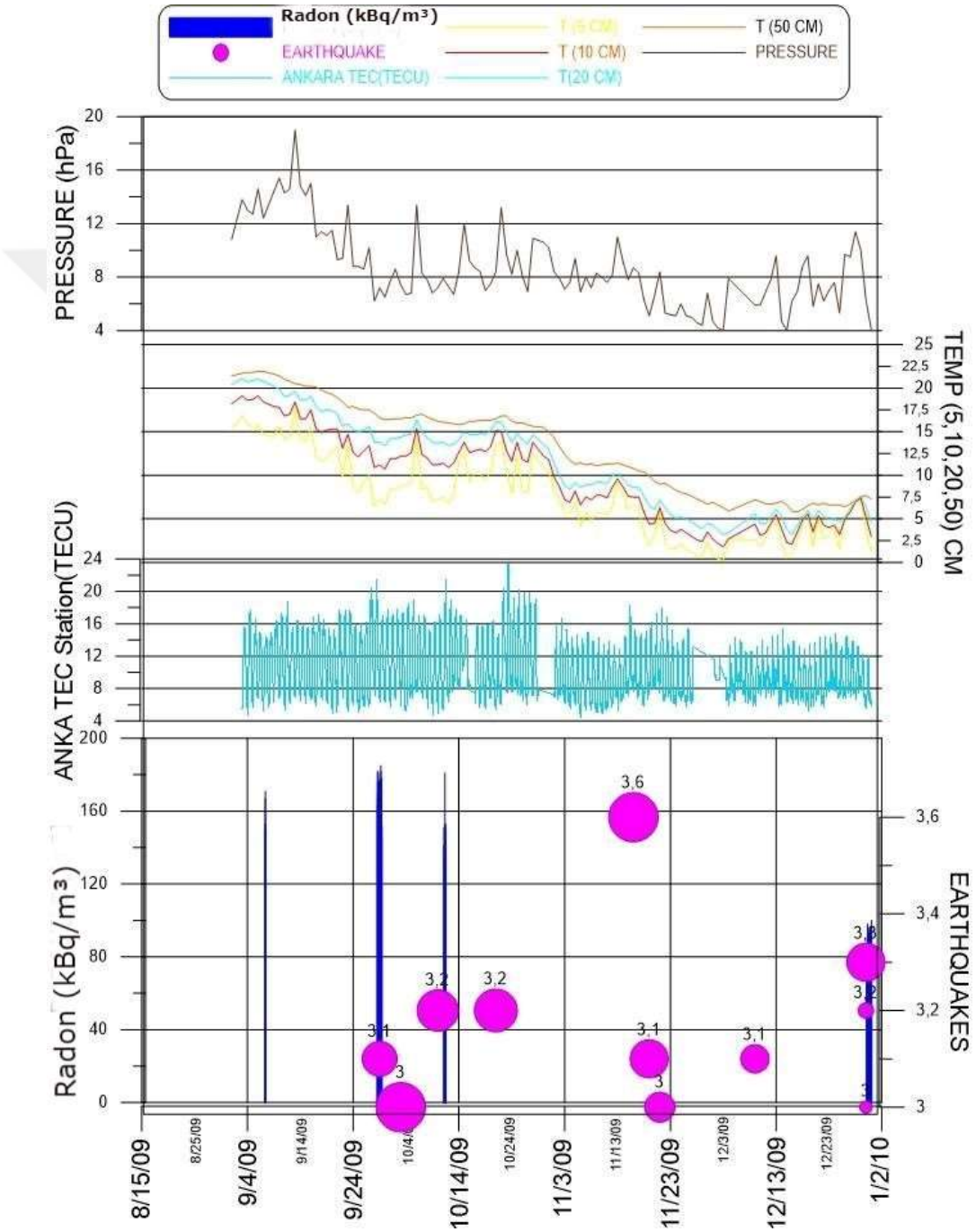

Figure 4.11. Radon, TEC, Temp of soil (5, 10, 20, and 50) cm and Pressure with Earthquakes for the Third group.

The four-point three earthquakes that accords in 2009 and seen in these figure have some little anomaly. Little Radon anomaly can only be dictated through another analysis. However, from these figure top panel we see that pressure was high to finish the earthquake and temperature was increasing and it was in one at twenty 20 cm, it shows an anomaly and then we see that Radon date was upset there is not available in Radon Date anomaly.

5. CONCLUSION

The relations between Earthquake-Total Electron Content-Radon were tried to be explained by ARIMA, Monte Carlo simulation method, and time series analysis. Seismo-Ionospheric Coupling studies have a critical place in earthquake predictions. In this study, we examined a triple change that was not previously studied in Seismo-Ionospheric studies. Many studies have been published on the relationship of soil Rn gas to earthquakes. Similarly, the changes caused by earthquakes in the ionosphere have been studied by a significant number of scientists. However, we could not find any studies that examined three variables. We think this research will be an important step to fill a critical gap in this area. The important results we have achieved can be listed as follows:

1. A positive interaction was observed between TEC-Rn and Earthquake,
2. Rn data at unknown times were successfully estimated with ARIMA and Monte Carlo Simulationmethod,
3. The meteorological data and TEC-Rn-Earthquake anomalies reacted positively,
4. In further studies, simulation methods can be further developed.

REFERENCES

[1] Nazaroff, W.W., Soil as a source of indoor radon: generation, migration, and entry. Radon and Its Decay Products in Indoor Air, 1988.

[2] Schumann, R. R., Owen, D. E., & Asher-Bolinder, S. (1988). Factors affecting soil-gas radon concentrations at a single site in the semiarid western us. In Proc. of the 1988 EPA Symposium on Radon and Radon Reduction Technology 2. Publication.

[3] Sextro, R. G., Moed, B. A., Nazaroff, W. W., Revzan, K. L., & Nero, A. V. (1987). Investigations of soil as a source of indoor radon.

[4] Okabe, S. (1956). Time variation of the atmospheric radon-content near the ground surface with relation to some geophysical phenomena. Memoirs of the College of Science, University of Kyoto. Series A, 28(2), 99-115.

[5] King, C. Y. (1980). Episodic radon changes in subsurface soil gas along active faults and possible relation to earthquakes. Journal of Geophysical Research: Solid Earth, 85(B6), 3065-3078.

[6] Birchard, G. F., & Libby, W. F. (1980). Soil radon concentration changes preceding and following four magnitude 4.2–4.7 earthquakes on the San Jacinto Fault in southern California. Journal of Geophysical Research: Solid Earth, 85(B6), 3100-3106.

[7] Shapiro, M. H., Melvin, J. D., Tombrello, T. A., Mendenhall, M. H., Larson, P. B., & Whitcomb, J. H. (1981). Relationship of the 1979 Southern California radon anomaly to a possible regional strain event. Journal of Geophysical Research: Solid Earth, 86(B3), 1725-1730.

[8] Rastogi, B. K., Chadha, R. K., & Raju, I. P. (1986). Seismicity near Bhatsa reservoir, Maharashtra, India. Physics of the earth and planetary interiors, 44(2), 179-199.

[9] Zmazek, B., Todorovski, L., Džeroski, S., Vaupotič, J., & Kobal, I. (2003). Application of decision trees to the analysis of soil radon data for earthquake prediction. Applied Radiation and Isotopes, 58(6), 697-706.

[10] Walia, V., Su, T. C., Fu, C. C., & Yang, T. F. (2005). Spatial variations of radon and helium concentrations in soil-gas across the Shan-Chiao fault, Northern Taiwan. Radiation Measurements, 40(2-6), 513-516.

[11] Hartmann, J., & Levy, J. K. (2005). Hydrogeological and gasgeochemical earthquake precursors–A review for application. Natural Hazards, 34(3), 279-304.

[12] Singh, S., Jaishi, H. P., Tiwari, R. P., & Tiwari, R. C. (2016). A study of variation in soil gas concentration associated with earthquakes near Indo-Burma Subduction zone. Geoenvironmental Disasters, 3(1), 1-8.

[13] Yang, T. F., Walia, V., Chyi, L. L., Fu, C. C., Chen, C. H., Liu, T. K., ... & Lee, M. (2005). Variations of soil radon and thoron concentrations in a fault zone and prospective earthquakes in SW Taiwan. Radiation Measurements, 40(2-6), 496-502.

[14] Baykut, S., Akgül, T., İnan, S., & Seyis, C. (2010). Observation and removal of daily quasi-periodic components in soil radon data. Radiation Measurements, 45(7), 872-879.

[15] Sac, M. M., Harmansah, C., Camgoz, B., & Sozbilir, H. (2011). Radon monitoring as the earthquake precursor in fault line in Western Turkey. Ekoloji, 20(79), 93-98.

[16] Oh, Y. H., & Kim, G. (2015). A radon-thoron isotope pair as a reliable earthquake precursor. Scientific reports, 5(1), 1-6.

[17] H. S. Virk Baljinder Singh, 1994 , Radon recording of Uttarkashi earthquake, gyophysical research letters, pp. 737-740

[18] Virk, H. S., Walia, V., & Kumar, N. (2001). Radon/helium precursory signals of Chamoli earthquakes, Garhwal Himalaya, India. J. Geodyn, 31, 201-210.

[19] Walia, V., Virk, H. S., & Bajwa, B. S. (2006). Radon precursory signals for some earthquakes of magnitude> 5 occurred in NW Himalaya: An overview. Pure and Applied Geophysics, 163(4), 711-721.

[20] Ramola, R. C., Singh, M., Sandhu, A. S., Singh, S., & Virk, H. S. (1990). The use of radon as an earthquake precursor. INT. J. RADIAT. APPLIC. INSTRUM. PART E., 4(2), 275-287.

[21] Ramola, R. C., Prasad, Y., Prasad, G., Kumar, S., & Choubey, V. M. (2008). Soil-gas radon as seism tectonic indicator in Garhwal Himalaya. Applied Radiation and Isotopes, 66(10), 1523-1530.

[22] Chaudhuri, H., Barman, C., Iyengar, A. N. S., Ghose, D., Sen, P., & Sinha, B. (2013). Long range correlation in earthquake precursory signals. The European Physical Journal Special Topics, 222(3), 827-838.

[23] Laskar, I., Phukon, P., Goswami, A. K., Chetry, G., & Roy, U. C. (2011). A possible link between radon anomaly and earthquake. Geochemical Journal, 45(6), 439-446.

[24] Jaishi, H. P., Singh, S., Tiwari, R. P., & Tiwari, R. C. (2014). Analysis of soil radon data in earthquake precursory studies. Annals of Geophysics, 57(5), 0544.

[25] Jaishi, H. P., Singh, S., Tiwari, R. P., & Tiwari, R. C. (2014). Correlation of radon anomalies with seismic events along Mat fault in Serchhip District, Mizoram, India. Applied radiation and isotopes, 86, 79-84.

[26] Deb, A., Gazi, M., & Barman, C. (2016). Anomalous soil radon fluctuations–signal of earthquakes in Nepal and eastern India regions. Journal of Earth System Science, 125(8), 1657-1665.

[27] Riggio, A., & Santulin, M. (2015). Earthquake forecasting: a review of radon as seismic precursor. Bollettino di Geofisica Teorica ed Applicata, 56(2).

[28] Baskaran, M. (2016). Radon: A tracer for geological, geophysical and geochemical studies (Vol. 367). Basel: Springer.

[29] Scholz, C. H., Sykes, L. R., & Aggarwal, Y. P. (1973). Earthquake prediction: A physical basis. Science, 181(4102), 803-810.

[30] Anderson, O. L., & Grew, P. C. (1977). Stress corrosion theory of crack propagation with applications to geophysics. Reviews of Geophysics, 15(1), 77-104.

[31] King, C. Y. (1978). Radon emanation on San Andreas Fault. Nature, 271(5645), 516-519.

[32] Petraki, E., Nikolopoulos, D., Panagiotaras, D., Cantzos, D., Yannakopoulos, P., Nomicos, C., & Stonham, J. (2015). Radon-222: a potential short-term earthquake precursor. Journal of Earth Science & Climatic Change, 6(6), 1.

[33] İnan, S., Akgül, T., Seyis, C., Saatçılar, R., Baykut, S., Ergintav, S., & Baş, M. (2008). Geochemical monitoring in the Marmara region (NW Turkey): A search for precursors of seismic activity. Journal of Geophysical Research: Solid Earth, 113(B3).

[34] İnan, S., Kop, A., Çetin, H., Kulak, F., Pabuçcu, Z., Seyis, C., & Bodur, M. N. (2012). Seasonal variations in soil radon emanation: long-term continuous monitoring in light of seismicity. Natural hazards, 62(2), 575-591.

[35] Singh, M. A. N. W. I. N. D. E. R., Ramola, R. C., Singh, S. U. R. I. N. D. E. R., & Virk, H. S. (1988). The influence of meteorological parameters on soil gas radon. J. Assoc. Explore. Geophys, 9, 85-90.

[36] Cigolini, C., Poggi, P., Ripepe, M., Laiolo, M., Ciamberlini, C., Delle Donne, D., & Genco, R. (2009). Radon surveys and real-time monitoring at Stromboli volcano: Influence of soil temperature, atmospheric pressure and tidal forces on 222Rn degassing. Journal of Volcanology and Geothermal Research, 184(3-4), 381-388.

[37] International Atomic Energy Agency (2007). IAEA Safety Glossary: Terminology Used in Nuclear Safety and Radiation Protection. ISBN 9789201007070

[38] Ramola, R. C. (2010). Relation between spring water radon anomalies and seismic activity in Garhwal Himalaya. Acta Geophysica, 58(5), 814-827.

[39] Sahoo, S. K., Katlamudi, M., Shaji, J. P., Krishna, K. M., & Lakshmi, G. U. (2018). Influence of meteorological parameters on the soil radon (Rn 222) emanation in Kutch, Gujarat, India. Environmental monitoring and assessment, 190(3), 1-20.

[40] Chowdhury, S., Barman, C., Deb, A., Raha, S., & Ghose, D. (2019). Study of variation of soil radon exhalation rate with meteorological parameters in Bakreswar–Tantloi geothermal region of West Bengal and Jharkhand, India. Journal of Radio analytical and Nuclear Chemistry, 319(1), 23-32.

[41] Fujiyoshi, R., Sakamoto, K., Imanishi, T., Sumiyoshi, T., Sawamura, S., Vaupotic, J., & Kobal, I. (2006). Meteorological parameters contributing to variability in 222Rn activity concentrations in soil gas at a site in Sapporo, Japan. Science of the total environment, 370(1), 224-234.

[42] New York: United Nations (published 2010). p. 4. ISBN 978-92-1-142274-0. Retrieved 9 November 2012

[43] Przylibski, T. A., Wyłomańska, A., Zimroz, R., & Fijałkowska-Lichwa, L. (2015). Application of spectral decomposition of 222Rn activity concentration signal series measured in Niedźwiedzia Cave to identification of mechanisms responsible for different time-period variations. Applied Radiation and Isotopes, 104, 74-86.

[44] Kumar, A., Walia, V., Arora, B. R., Yang, T. F., Lin, S. J., Fu, C. C., ... & Wen, K. L. (2015). Identifications and removal of diurnal and semidiurnal variations in radon time series data of Hsinhua monitoring station in SW Taiwan using singular spectrum analysis. Natural Hazards, 79(1), 317-330.

[45] Huang, N. E., Shen, Z., Long, S. R., Wu, M. C., Shih, H. H., Zheng, Q., ... & Liu, H. H. (1998). The empirical mode decomposition and the Hilbert spectrum for nonlinear and non-stationary time series analysis. Proceedings of the Royal Society of London. Series A: mathematical, physical and engineering sciences, 454(1971), 903-995.

[46] Jha, R., Raju, D., & Sen, A. (2006). Analysis of tokamak data using a novel Hilbert transform based technique. Physics of plasmas, 13(8), 082507.

[47] Wharton, A. M., Sekar Iyengar, A. N., & Janaki, M. S. (2013). Study of nonlinear oscillations in a glow discharge plasma using empirical mode decomposition and Hilbert Huang transform. Physics of Plasmas, 20(2), 022301.

[48] Spanos, P. D., Giaralis, A., & Politis, N. P. (2007). Time–frequency representation of earthquake accelerograms and inelastic structural response records using the adaptive chirplet decomposition and empirical mode decomposition. Soil Dynamics and Earthquake Engineering, 27(7), 675-689.

[49] Yu, D. J., & Ren, W. X. (2005). EMD-based stochastic subspace identification of structures from operational vibration measurements. Engineering Structures, 27(12), 1741-1751.

[50] Echeverria, J. C., Crowe, J. A., Woolfson, M. S., & Hayes-Gill, B. R. (2001). Application of empirical mode decomposition to heart rate variability analysis. Medical and Biological Engineering and Computing, 39(4), 471-479.

[51] Wu, M. C., & Hu, C. K. (2006). Empirical mode decomposition and synchrogram approach to cardiorespiratory synchronization. Physical Review E, 73(5), 051917.

[52] Ionizing radiation exposure of the population of the United States. Bethesda, Md.: National Council on Radiation Protection and Measurements. 2009. ISBN 978-0-929600-98-7. NCRP No. 160

[53] Crockett, R. G., & Gillmore, G. K. (2010). Spectral-decomposition techniques for the identification of radon anomalies temporally associated with earthquakes occurring in the UK in 2002 and 2008. Natural Hazards and Earth System Sciences, 10(6), 1079-1084.

[54] Crockett, R. G., Perrier, F., & Richon, P. (2010). Spectral-decomposition techniques for the identification of periodic and anomalous phenomena in radon time-series. Natural Hazards and Earth System Sciences, 10(3), 559-564.

[55] Barman, C., Ghose, D., Sinha, B., & Deb, A. (2016). Detection of earthquake induced radon precursors by Hilbert Huang Transform. Journal of Applied Geophysics, 133, 123-131.

[56] Chowdhury, S., Deb, A., Nurujjaman, M., & Barman, C. (2017). Identification of pre-seismic anomalies of soil radon-222 signal using Hilbert–Huang transform. Natural Hazards, 87(3), 1587-1606.

[57] Ministry of Education, Culture, Sports, Science, and Technology of Japan "Radiation in environment" retrieved 2011-6-29

[58] Darby; et al. (January 29, 2005). "Radon in homes and risk of lung cancer: collaborative analysis of individual data from 13 European case-control studies"

[59] Temuujin, J., Surenjav, E., Ruescher, C. H., & Vahlbruch, J. (2019). Processing and uses of fly ash addressing radioactivity (critical review). Chemosphere, 216, 866-882.

[60] Keith, S., Doyle, J. R., Harper, C., Mumtaz, M., Tarrago, O., Wohlers, D. W., & Barber, L. E. (2012). GLOSSARY. In Toxicological Profile for Radon. Agency for Toxic Substances and Disease Registry (US).

[61] Morewitz, S. J. (2014). Sociological Theory and Methods in Toxic Tort Lawsuits. In Handbook of Forensic Sociology and Psychology (pp. 281-304). Springer, New York, NY.

[62] Vanchieri, C. (1990). Radiation Therapy Pursuit Leads to Unearthing of “Hot Bones”.

[63] Keith, S., Doyle, J. R., Harper, C., Mumtaz, M., Tarrago, O., Wohlers, D. W., ... & Barber, L. E. (2012). GLOSSARY. In Toxicological Profile for Radon. Agency for Toxic Substances and Disease Registry (US).

[64] Porstendörfer, J., Butterweck, G., & Reineking, A. (1994). Daily variation of the radon concentration indoors and outdoors and the influence of meteorological parameters. Health physics, 67(3), 283-287.

[65] Bartoli, G., Carraturo, N., Gargiulo, E., Parrella, A., & Santi, B. (1989). Evaluation of the exposure levels to radioactivity in the hot-spring environment of the Island of Ischia during a year. Annali di igiene: medicina preventiva e di comunita, 1(6), 1781-1823.

[66] "Predicted median annual-average living-area concentration, by county". Lawrence Berkeley National Laboratory. Archived from the original on 2007-12-31. Retrieved 2008-02-12.

[67] Yamamoto, M., Sakaguchi, A., Sasaki, K., Hirose, K., Igarashi, Y., & Kim, C. K. (2006). Seasonal and spatial variation of atmospheric 210Pb and 7Be deposition: features of the Japan Sea side of Japan. Journal of Environmental Radioactivity, 86(1), 110-131.

[68] "Basic Information about Radon in Drinking Water". United States Environmental Protection Agency. June 30, 2014. Archived from the original on 2015-02-14. Retrieved January 31, 2015.

[69] Yamazawa, H., Matsuda, M., Moriizumi, J., & Iida, T. (2008, August). Wet Deposition of Radon Decay Products and its Relation with Long-Range Transported Radon. In AIP Conference Proceedings (Vol. 1034, No. 1, pp. 149-152). American Institute of Physics.

[70] Greenfield, M. B., Iwata, A., Ito, N., Ishigaki, M., Kubo, K., & Komura, K. (2006, October). Intense γ radiation from radon progeny accreted in/on rain during and following thunderstorms. In APS Division of Nuclear Physics Meeting Abstracts (pp. BH-005).

[71] Greenfield, M. B., Ito, N., Iwata, A., Kubo, K., Ishigaki, M., & Komura, K. (2008). Determination of rain age via γ rays from accreted radon progeny. Journal of Applied Physics, 104(7), 074912.

[72] Valevech, A. D., & Shepeleva, A. E. (2010). Radium and Radon in the Environment. Modern Technique and Technologies MTT'2010, 86, 172.

[73] Gottlieb, L. S., & Husen, L. A. (1982). Lung cancer among Navajo uranium miners. Chest, 81(4), 449-452.

[74] POLICY, C., & JUSTICE, C. (2005). Examining Possible Causes of Gulf War Illness.

[75] Denman, A. R., Eatough, J. P., Gillmore, G., & Phillips, P. S. (2003). Assessment of health risks to skin and lung of elevated radon levels in abandoned mines. Health physics, 85(6), 733-739.

[76] Hala, J. (1998). Radioactivity, ionizing radiation, nuclear energy.

[77] Bolck, F. (1990). Man-Made Mineral Fiber's and Radon IARC Monographs on the Evaluation of Carcinogenic Risks to Humans, Vol. 43 World Health Organization, International Agency for Research on Cancer, IARC, Lyon, France (1988), ISBN: 9283212436 300 pages, Sw. fr. 65.-/US $52.00.

[78] Samet, J. M. (1992). Indoor radon and lung cancer. Estimating the risks. Western journal of medicine, 156(1), 25.

[79] "The Radon Story". The Radon Council. 2001. Archived from the original on February 1, 2015. Retrieved January 1, 2015.

[80] Boyd, David R. (2006). "Radon The Unfamiliar Killer". Healthy Environment, Healthy Canadians Series, Report No.1. Vancouver: David Suzuki Foundation. Retrieved February 1, 2015.

[81] Roessler, C. E., Morato, R., Richards, R., Mohammed, H., & Hintenlang, D. E. (1995). Design and testing of sub-slab depressurization for radon mitigation in north Florida houses. Part 1. Performance and durability. Volume 2. Data appendices. Final report, August 1988-December 1990 (No. PB-96-103593/XAB). Florida Univ., Gainesville, FL (United States).

[82] Field, R. W. (2018). Radon: A leading environmental cause of lung cancer. American family physician, 98(5), 280-282.

[83] Williams, David R. (2007-04-19). "Earth Fact Sheet". NASA. Retrieved 2008-06-26.

[84] Clark, D. L., Neu, M. P., Runde, W., & Keogh, D. W. (2000). Uranium and uranium compounds. Kirk-Othmer Encyclopedia of Chemical Technology.

[85] Ahmed, H. A. (2010). Investigation of indoor radon concentration in block houses in Omderman.

[86] Saito, M., Takata, S., Yamazawa, N., & Horiuchi, K. (1999). Determination of radon solubilities to 1, 2-Dimethylbenzene, 1, 3-Dimethylbenzene, 1, 4-Dimethylbenzene, 1, 3, 5-Trimethylbenzene, 1, 2, 4-Trimethylbenzene and 1-Isopropyl-4-methylbenzene. Nippon Kagaku Kaishi, 1999(6), 363-368.

[87] Keller, C., Wolf, W., & Shani, J. (2000). Radionuclides, 2. Radioactive Elements and Artificial Radionuclides. Ullmann's Encyclopedia of Industrial Chemistry.

[88] Bader, R. F. (1970). An introduction to the electronic structure of atoms and molecules. Clarke, Irwin.

[89] Lide, D. R. (2003). Atomic, molecular, and optical physics; ionization potentials of atoms and atomic ions. CRC handbook of chemistry and physics.

[90] Avrorin, V. V., Krasikova, R. N., Nefedov, V. D., & Toropova, M. A. (1982). The chemistry of radon. Russian Chemical Reviews, 51(1), 12.

[91] Stein, L. (1970). Ionic radon solutions. Science, 168(3929), 362-364.

[92] Pitzer, K. S. (1975). Fluorides of radon and element 118.

[93] Lawrence, S. (1983). The Chemistry of radon. Radiochemical Acta 32H63-17n.

[94] Liao, M. S., & Zhang, Q. E. (1998). Chemical bonding in XeF2, XeF4, KrF2, KrF4, RnF2, XeCl2, and XeBr2: from the gas phase to the solid state. The Journal of Physical Chemistry A, 102(52), 10647-10654.

[95] Filatov, M., & Cremer, D. (2003). Bonding in radon hexafluoride: An unusual relativistic problem? Physical Chemistry Chemical Physics, 5(6), 1103-1105.

[96] Holloway, J. H. (1986). Noble-gas fluorides. Journal of fluorine chemistry, 33(1-4), 149-158.

[97] Avrorin, V. V., Krasikova, R. N., Nefedov, V. D., & Toropova, M. A. (1982). The chemistry of radon. Russian Chemical Reviews, 51(1), 12.

[98] Holloway, J. H., & Hope, E. G. (1998). Recent advances in noble-gas chemistry. Advances in Inorganic Chemistry, 46, 51-100.

[99] Thayer, J. S. (2010). Relativistic effects and the chemistry of the heavier main group elements. Relativistic methods for chemists, 63-97.

[100] Liebman, J. F. (1975). Conceptual problems in noble gas and fluorine chemistry, II: The nonexistence of radon tetrafluoride. Inorganic and Nuclear Chemistry Letters, 11(10), 683-685.

[101] Seppelt, K. (2015). Molecular hexafluorides. Chemical Reviews, 115(2), 1296-1306.

[102] Malli, G. L. (2002). Prediction of the existence of radon carbonyl: RnCO. International journal of quantum chemistry, 90(2), 611-615.

[103] Runeberg, N., & Pyykkö, P. (1998). Relativistic pseudopotential calculations on Xe2, RnXe, and Rn2: The van der Waals properties of radon. International journal of quantum chemistry, 66(2), 131-140.

[104] Browne, Malcolm W. (1993). "Chemists Find Way to Make An 'Impossible' Compound". The New York Times. Retrieved 2009-01-30.

[105] Dolg, M., Küchle, W., Stoll, H., Preuss, H., & Schwerdtfeger, P. (1991). Ab initio pseudopotentials for Hg to Rn: II. Molecular calculations on the hydrides of Hg to At and the fluorides of Rn. Molecular Physics, 74(6), 1265-1285.

[106] Sonzogni, A. (2008). Interactive chart of nuclides. National Nuclear Data Center: Brookhaven National Laboratory. Retrieved, 6.

[107] Kozempel, J. (2017). Radon Nuclides and Radon Generators. Radon, 7.

[108] "Principal Decay Scheme of the Uranium Series". Gulflink.osd.mil. Archived from the original on 2008-10-25. Retrieved 2008-09-12.

[109] Rutherford, E., & Owens, R. B. (1899). Thorium and uranium radiation. Roy. soc. of Canada.

[110] Partington, J. R. (1957). Discovery of radon. Nature, 179(4566), 912-912.

[111] Schüttmann, W. (1988). Zur Entdeckungsgeschichte des Radons.

[112] Brenner, D. J. (2000). Rutherford, the Curies, and radon. Medical Physics-Lancaster PA-, 27(3), 618-618.

[113] Curie, P., & Curie, M. (1899). Sur la radioactivité provoquée par les rayons de Becquerel. Gauthier-Villars.

[114] Dorn, E. (1901). Uber die von radioaktiven substanzen ausgesandte emanation. Abhandlung der Naturforschung. Gesellschaft zur Halle, 23, 1-15.

[115] Baskaran, M. (2016). Physical, Chemical and Nuclear Properties of Radon: An Introduction. In Radon: A Tracer for Geological, Geophysical and Geochemical Studies (pp. 1-14). Springer, Cham.

[116] Rayner-Canham, M., & Rayner-Canham, G. (2019). Harriet Brooks: radon, a ‘new gas’ from radium. Women in their elements: Selected women’s contributions to the periodic system. Singapore: World Scientific, 269-279.

[117] Giesel, F. (1903). Ueber den Emanationskörper aus Pechblende und über Radium. Berichte der deutschen chemischen Gesellschaft, 36(1), 342-347.

[118] Debierne, A. (1903). Sur la radio-activité induite provoquée par les sels d’actinium. R, 136, 446-449.

[119] Schmidt, C. (1918). Periodisches System und Genesis der Elemente. Zeitschrift für anorganische und allgemeine Chemie, 103(1), 79-118.

[120] Perrin, J. (1919). Matiere et lumiere-Essai de synthese de la mécanique chimique. In Annales de Physique (Vol. 9, No. 11, pp. 5-108). EDP Sciences.

[121] Adams, E. Q. (1920). The Independent Origin of Actinium. Journal of the American Chemical Society, 42(11), 2205-2208.

[122] Ramsay, W., & Collie, J. N. (1904). The spectrum of the radium emanation. Proceedings of the Royal Society of London, 73(488), 470-476.

[123] Robbins, K. B., Brandling-Bennett, D., & Hinman, A. R. (1981). Low measles incidence: association with enforcement of school immunization laws. American Journal of Public Health, 71(3), 270-274.

[124] Klein, E., Klein, G., Nadkarni, J. S., Nadkarni, J. J., Wigzell, H., & Clifford, P. (1968). Surface IgM-kappa specificity on a Burkitt lymphoma cell in vivo and in derived culture lines. Cancer research, 28(7), 1300-1310.

[125] Gray, R. W., & Ramsay, W. (1909). CXXII.—some physical properties of radium emanation. Journal of the Chemical Society, Transactions, 95, 1073-1085.

[126] Ramsay, W., & Gray, R. W. (1910). La densité de l'émanation du Radium. Comptes rendus hebdomadaires des séances de l'Académie de Sciences, 151, 126-128.

[127] Thornton, B. F., & Burdette, S. C. (2013). Recalling radon's recognition. Nature chemistry, 5(9), 804-804.

[128] Grosse, A. V. (1965). Some physical and chemical properties of element 118 (Eka-Em) and element 86 (Em). Journal of Inorganic and Nuclear Chemistry, 27(3), 509-519.

[129] Fields, P. R., Stein, L., & Zirin, M. H. (1962). Radon fluoride. Journal of the American Chemical Society, 84(21), 4164-4165.

[130] Upfal, M., Wigington, P. S., & Harris, B. (2000). Radon toxicity.

[131] Proctor, R. (2000). The Nazi war on cancer. Princeton University Press.

[132] Edelstein, M. R., & Makofske, W. J. (1998). Radon's deadly daughters: science, environmental policy, and the politics of risk. Rowman & Littlefield.

[133] Samet, J. M. (1992). Indoor radon and lung cancer. Estimating the risks. Western journal of medicine, 156(1), 25.

[134] The Clinique, Volume 34. Illinois Homeopathic Medical Association. 1913. Retrieved 2011-06-30.

[135] Graham, J., Burstein, P., & Kurohara, S. S. (1968). Incidence of Second Cancers After Radon Seed Therapy for Cervix Cancer. Acta radiologica: therapy, physics, biology, 7(6), 453-461.

[136] Néda, T., Szakács, A., Mócsy, I., & Cosma, C. (2008). Radon concentration levels in dry CO2 emanations from Harghita Băi, Romania, used for curative purposes. Journal of Radioanalytical and Nuclear Chemistry, 277(3), 685-691.

[137] Salak, K., & Nordeman, L. (2004). 59631, Mining for Miracles. National Geographic Jan, 2004, 118-122.

[138] Richon, P., Klinger, Y., Tapponnier, P., Li, C. X., Van Der Woerd, J., & Perrier, F. (2010). Measuring radon flux across active faults: Relevance of excavating and possibility of satellite discharges. Radiation Measurements, 45(2), 211-218.

[139] Semprini, L., & Kruger, P. (1980, January). Radon Transect Analysis In Geothermal Reservoirs. In SPE California Regional Meeting. Society of Petroleum Engineers.

[140] Igarashi, G., & Wakita, H. (1995). Geochemical and Hydrological Observations for arthquake Prediction in Japan. Journal of Physics of the Earth, 43(5), 585-598.

[141] Tsunogai, U., & Wakita, H. (1996). Anomalous Changes in Groundwater Chemistry Possible Precursors of the 1995 Hyogo-ken Nanbu Earthquake, Japan. Journal of Physics of the Earth, 44(4), 381-390.

[142] Richon, P., Sabroux, J. C., Halbwachs, M., Vandemeulebrouck, J., Poussielgue, N., Tabbagh, J., & Punongbayan, R. (2003). Radon anomaly in the soil of Taal volcano, the Philippines: A likely precursor of the M 7.1 Mindoro earthquake (1994). Geophysical Research Letters, 30(9).

[143] Kovler, K., Perevalov, A., Steiner, V., & Metzger, L. A. (2005). Radon exhalation of cementitious materials made with coal fly ash: Part 1–scientific background and testing of the cement and fly ash emanation. Journal of environmental radioactivity, 82(3), 321-334.

[144] Battye, D. L., & Ashman, P. J. (2009). Radiation associated with Hot Rock geothermal power. In Proceedings of the 2009 Australian Geothermal Energy Conference, Geoscience Australia, Record (Vol. 35).

[145] JAT, D. (1946). Radon. Its Properties and Preparation for Industrial Radiography.

[146] Morrison, A. (1945). Use of radon for industrial radiography. Canadian journal of research, 23(6), 413-419.

[147] Fleischer, R. L., & Mogro-Campero, A. (1978). Mapping of integrated radon emanation for detection of long-distance migration of gases within the Earth: Techniques and principles. Journal of Geophysical Research: Solid Earth, 83(B7), 3539-3549.

[148] Iimasti, V. (1987). Device for measuring radon gas concentration. Finnish Patent, (002), 717.

[149] Abdalla, A. M., Ismail, A. M., & Al-Naggar, T. I. (2017). Radon Calibration System. Radon, 125.

[150] United Nations Scientific Committee on the Effects of Atomic Radiation. (1982). Ionizing radiation: sources and biological effects. 1982 report to the general assembly, with annexes.

[151] United Nations Scientific Committee on the Effects of Atomic Radiation. (1988). Sources, effects and risks of ionizing radiation.

[152] International Commission on Radiological Protection. (1977). Recommendations of the international commission on radiological protection (No. 26). Elsevier Science & Technology.

[153] Abu-Jarad, F., & Fremlin, J. H. (1983). Effect of internal wall covers on radon emanation inside houses. Health physics, 44(3), 243-248.

[154] Minkin, L. (2002). Is diffusion, thermos diffusion, or advection a primary mechanism of indoor radon entry? Radiation protection dosimetry, 102(2), 153-161.

[155] Shweikani, R., Giaddui, T. G., & Durrani, S. A. (1995). The effect of soil parameters on the radon concentration values in the environment. Radiation measurements, 25(1-4), 581-584.

[156] Gundersen, L. (1992). The effect of rock type, grain size, sorting, permeability, and moisture on measurements of radon in soil gas: A comparison of two measurement techniques. Journal of radio analytical and nuclear chemistry, 161(2), 325-337.

[157] Mazur, D., Janik, M., Łoskiewicz, J., Olko, P., & Swakoń, J. (1999). Measurements of radon concentration in soil gas by CR-39 detectors. Radiation Measurements, 31(1-6), 295-300.

[158] Albarracin, D., Font, L., Amgarou, K., Domingo, C., Fernandez, F., & Baixeras, C. (2002). Effect of soil parameters on radon entry into a building by means of the TRANSRAD numerical model. Radiation protection dosimetry, 102(4), 359-363.

[159] Fleischer, R. L., & Mogro-Campero, A. (1978). Mapping of integrated radon emanation for detection of long-distance migration of gases within the Earth: Techniques and principles. Journal of Geophysical Research: Solid Earth, 83(B7), 3539-3549.

[160] Singh, H. B., Salas, L. J., Chatfield, R. B., Czech, E., Fried, A., Walega, J., ... & Fuelberg, H. (2004). Analysis of the atmospheric distribution, sources, and sinks of oxygenated volatile organic chemicals based on measurements over the Pacific during TRACE-P. Journal of Geophysical Research: Atmospheres, 109(D15).

[161] Lide, D. R. (Ed.). (2004). CRC handbook of chemistry and physics (Vol. 85). CRC press.

[162] Vázquez, M., & Hanslmeier, A. (2005). Ultraviolet radiation in the solar system (Vol. 331). Springer Science & Business Media.

[163] Jones, D. (1917). Peter Roach, James Hartmann and Jane Setter, eds. English Pronouncing Dictionary.

[164] Murphy, A. J. (1994). Book reviews--Merriam-Webster's Collegiate Dictionary. Technical Communication, 41(4), 732.

[165] Hardwick, M. (2020). What the Universe Tells Us about God and Christian Apologetics (Doctoral dissertation, Regent University).

[166] Rabiu, U. C., Onimisi, A. B., & Achem, M. Y. (2013). Using Locally Generated Magnetic Indices to Characterize the Ionosphere From Magnetic Data Acquisition System (Magdas) Ground Based Observatories in Nigeria. European Journal of Sustainable Development, 2(2), 177-177.

[167] Belrose, J. S. (2004). Marconi and the History of Radio. IEEE Antennas and Propagation Magazine, 46(2), 130-131.

[168] Bond, G. E. (1997). The interaction of radio waves with the auroral ionosphere (Doctoral dissertation, University of Leicester).

[169] Rigney, L. I. (2001). A first perspective of Indigenous Australian participation in science: Framing Indigenous research towards Indigenous Australian intellectual sovereignty.

[170] Fremouw, E. J. (1986). The Polar Bear Ionospheric Experiments. A Pre-Launch Overview. Physical Dynamics Inc Bellevue Wa.

[171] Kelley, M. C. (2009). The Earth's ionosphere: plasma physics and electrodynamics. Academic press.

[172] Liu, J. Y., Tsai, H. F., & Jung, T. K. (1996). Total electron content obtained by using the global positioning system. Terrestrial, Atmospheric and Oceanic Sciences, 7(1), 107-117.

[173] Rama Rao, P. V. S., Gopi Krishna, S., Niranjan, K., & Prasad, D. S. V. V. D. (2006, December). Temporal and spatial variations in TEC using simultaneous measurements from the Indian GPS network of receivers during the low solar activity period of 2004–2005. In Annales Geophysicae (Vol. 24, No. 12, pp. 3279-3292). Copernicus GmbH.

[174] Lichtenegger, H., Hofmann-Wellenhof, B., & Collins, J. (1997). Global Positioning System: Theory and Practice. Springer.

[175] Rawer, K., Lincoln, J. V., & Conkright, R. O. (1981). International Reference Ionosphere–IRI 79. World Data Center A for Solar-Terrestrial Physics, Report UAG-82, Boulder, Colorado, 245, 245.

[176] Bilitza, D. (1997). International reference ionosphere—status 1995/96. Advances in Space Research, 20(9), 1751-1754.

[177] Bilitza, D. (2001). International reference ionosphere 2000. Radio Science, 36(2), 261-275.

[178] Iyer, K. N., Joshi, H. P., Jivrajani, R. D., & Aravindakshan, P. (1996). Comparative study of TEC near the crest of the equatorial anomaly with IRI model for solar minimum to solar maximum. Advances in Space Research, 18(6), 233-236.

[179] Irlapati, G. R. GR Irlapati's Geoscope (1987).

[180] Allen, C. R., Edwards, W., Hall, W. J., Knopoff, L., Raleigh, C. B., Savit, C. H., ... & Turner, R. H. (1976). Predicting earthquakes: a scientific and technical evaluation-with implications for society. Panel on Earthquake Prediction of the Committee on Seismology, Assembly of Mathematical and Physical Sciences, National Research Council, US National Academy of Sciences, Washington, DC, 1-4.

[181] Uyeda, S., Nagao, T., & Kamogawa, M. (2009). Short-term earthquake prediction: Current status of seismo-electromagnetics. Tectonophysics, 470(3-4), 205-213.

[182] Console, R. (2001). Testing earthquake forecast hypotheses. Tectonophysics, 338(3-4), 261-268.

[183] Geller, R. J. (1997). Earthquake prediction: a critical review. Geophysical Journal International, 131(3), 425-450.

[184] Sharples, R. W., Huby, P. M., & Fortenbaugh, W. W. (Eds.). (1994). Theophrastus of Eresus: Sources on biology (Vol. 64). Brill.

[185] Cicerone, R. D., Ebel, J. E., & Britton, J. (2009). A systematic compilation of earthquake precursors. Tectonophysics, 476(3-4), 371-396.

[186] Khan, A. A. (2018). The geo-genetic status of earthquake-related hazards and the role of human and policy dimensions in impact mitigation. Environmental Hazards, 17(4), 276-291.

[187] Wyss, M., & Booth, D. C. (1997). The IASPEI procedure for the evaluation of earthquake precursors. Geophysical Journal International, 131(3), 423-424.

[188] Marzocchi, W., Papadopoulos, G., Sobolev, G., Yamaoka, K., & Zschau, J. Operational Earthquake Forecasting: State of knowledge and guidelines for utilization. Ann. Geophys, 54, 315391.

[189] Bordikar, M. R. (2013). *Analysis of Plasma Wave Irregularities Generated during Active Experiments in Near-Earth Space Environment* (Doctoral dissertation, Virginia Tech).

[190] Evans, J. V. (1969). Theory and practice of ionosphere study by Thomson scatter radar. *Proceedings of the IEEE*, *57*(4), 496-530.

[191] Alexander, D. E. (2014). Communicating earthquake risk to the public: the trial of the "L'Aquila Seven". Natural Hazards, 72(2), 1159-1173.

[192] Cicerone, R. D., Ebel, J. E., & Britton, J. (2009). A systematic compilation of earthquake precursors. Tectonophysics, 476(3-4), 371-396.

[193] Hough, S. E. (2016). Predicting the unpredictable: the tumultuous science of earthquake prediction. Princeton University Press.

[194] Johnston, M. J. S. (2002). Electromagnetic fields generated by earthquakes. International Geophysics Series, 81(A), 621-636.

[195] Park, S. K. (1996). Precursors to earthquakes: seism electromagnetic signals. Surveys in Geophysics, 17(4), 493-516.

[196] Geller, R. (1996). Electron cyclotron resonance ion sources and ECR plasmas. CRC Press.

[197] Park, S. K., Dalrymple, W., & Larsen, J. C. (2007). The 2004 Parkfield earthquake: Test of the electromagnetic precursor hypothesis. Journal of Geophysical Research: Solid Earth, 112(B5).

[198] Main, I. G., Bell, A. F., Meredith, P. G., Geiger, S., & Touati, S. (2012). The dilatancy–diffusion hypothesis and earthquake predictability. Geological Society, London, Special Publications, 367(1), 215-230.

[199] Lister, C. R. B. (1974). On the penetration of water into hot rock. Geophysical Journal International, 39(3), 465-509.

[200] Hammond, A. L. (1974). Dilatancy: Growing acceptance as an earthquake mechanism. Science, 184(4136), 551-552.

[201] Scholz, C. H. (1973). The physical basis for earthquake prediction. Science, 181, 803-810.

[202] McEvilly, T. V., & Johnson, L. R. (1974). Stability of P an S velocities from Central California quarry blasts. Bulletin of the Seismological Society of America, 64(2), 343-353.

[203] Lindh, A. G., Lockner, D. A., & Lee, W. H. K. (1978). Velocity anomalies: An alternative explanation. Bulletin of the Seismological Society of America, 68(3), 721-734.

[204] Freund, F. (2000). Time-resolved study of charge generation and propagation in igneous rocks. Journal of Geophysical Research: Solid Earth, 105(B5), 11001-11019.

[205] Hough, S. E. (2016). Predicting the unpredictable: the tumultuous science of earthquake prediction. Princeton University Press.

[206] Heraud, J. A., Centa, V. A., & Bleier, T. (2015, December). Electromagnetic Precursors Leading to Triangulation of Future Earthquakes and Imaging of the Subduction Zone. In AGU Fall Meeting Abstracts (Vol. 2015, pp. NH32B-03).

[207] Freund, F. T., Takeuchi, A., & Lau, B. W. (2006). Electric currents streaming out of stressed igneous rocks–A step towards understanding pre-earthquake low frequency EM emissions. Physics and Chemistry of the Earth, Parts A/B/C, 31(4-9), 389-396.

[208] Freund, F. T., Kulahci, I. G., Cyr, G., Ling, J., Winnick, M., Tregloan-Reed, J., & Freund, M. M. (2009). Air ionization at rock surfaces and pre-earthquake signals. Journal of Atmospheric and Solar-Terrestrial Physics, 71(17-18), 1824-1834.

[209] Eftaxias, K., Balasis, G., Contoyiannis, Y., Papadimitriou, C., Kalimeri, M., Athanasopoulou, L., & Nomicos, C. (2010). Unfolding the procedure of characterizing recorded ultra-low frequency, kHZ and MHz electromagnetic anomalies prior to the L'Aquila earthquake as pre-seismic ones-Part 2. Natural Hazards and Earth System Sciences, 10(2), 275-294.

[210] Tsolis, G. S., & Xenos, T. D. (2010). A qualitative study of the seismo-ionospheric precursors prior to the 6 April 2009 earthquake in L'Aquila, Italy. Natural Hazards and Earth System Sciences, 10(1), 133-137.

[211] Rozhnoi, A., Solovieva, M., Molchanov, O., Schwingenschuh, K., Boudjada, M., Biagi, P. F., & Hayakawa, M. (2009). Anomalies in VLF radio signals prior the Abruzzo earthquake (M= 6.3) on 6 April 2009. Natural Hazards and Earth System Sciences, 9(5), 1727-1732.

[212] Biagi, P. F., Maggipinto, T., Righetti, F., Loiacono, D., Schiavulli, L., Ligonzo, T., & Contadakis, M. E. (2011). The European VLF/LF radio network to search for earthquake precursors: setting up and natural/man-made disturbances. Natural Hazards and Earth System Sciences, 11(2), 333-341.

[213] Politis, D., Potirakis, S. M., & Hayakawa, M. (2020). Criticality analysis of 3-year-long VLF subionospheric propagation data possibly related to significant earthquake events in Japan. Natural Hazards, 102(1), 47-66.

[214] Gautam, A., Jha, J., & Singh, A. K. (2020). Modeling and forecasting of confirmed and recovered cases of COVID-19 in India. International Journal of Academic Medicine, 6(2), 83.

[215] Hyndman, R. J., & Athanasopoulos, G. (2015). 8.9 Seasonal ARIMA models. Forecasting: principles and practice. Texts. Retrieved, 19.

[216] Hamilton, J. D. (2020). Time series analysis. Princeton university press.

[217] PAPOULIS, A., & PILLAI, S. (2002). Unnikrishna: Probability. Random Variables and Stochastic Processes, Fourth Edition. sl: McGraw-Hill.

[218] Wang, S., Li, C., & Lim, A. (2019). Why are the ARIMA and SARIMA not sufficient. arXiv preprint arXiv:1904.07632.

[219] Box, G. E., Jenkins, G. M., Reinsel, G. C., & Ljung, G. M. (2015). Time series analysis: forecasting and control. John Wiley & Sons.

[220] Leonard, M. J., Chipley, M. R., Ambulgekar, K., Mainkar, S. A., Dixit, A. B., Shrotriya, S., ... & Apte, D. P. (2015). U.S. Patent No. 9,037,998. Washington, DC: U.S. Patent and Trademark Office.

[221] Zhang, G. P. (2003). Time series forecasting using a hybrid ARIMA and neural network model. Neurocomputing, 50, 159-175.

[222] Box, G. E., Jenkins, G. M., Reinsel, G. C., & Ljung, G. M. (2015). Time series analysis: forecasting and control. John Wiley & Sons.

[223] Rizkya, I., Syahputri, K., Sari, R. M., Siregar, I., & Utaminingrum, J. (2019, August). Autoregressive Integrated Moving Average (ARIMA) Model of Forecast Demand in Distribution Centre. In IOP Conference Series: Materials Science and Engineering (Vol. 598, No. 1, p. 012071). IOP Publishing.

[224] Wei, W. W. S., & Wei, W. W. S. (1990). Intervention analysis and outlier detection. Time series analysis: univariate and multivariate methods. Redwood City, California, USA: Addison-Wesley Pub, 184-195.

[225] Cabahug, C. O. (2007). Stochastic ARIMA modelling with white noise characteristic of electrical frequency uctuations in Mindanao. B.S.Thesis, MSU-Iligan Institute of Technology, Iligan, Philippines.

[226] Box, G. E., Jenkins, G. M., & Reinsel, G. C. (1994). Time series analysis, forecasting and control. Englewood Clifs.

[227] Burns, P. (2002). Robustness of the Ljung-Box test and its rank equivalent. Available at SSRN 443560.

[228] Lee, C. K., Song, H. J., & Mjelde, J. W. (2008). The forecasting of International Expo tourism using quantitative and qualitative techniques. Tourism management, 29(6), 1084-1098.

[229] Tordecilla, R. D., Juan, A. A., Montoya-Torres, J. R., Quintero-Araujo, C. L., & Panadero, J. (2021). Simulation-optimization methods for designing and assessing resilient supply chain networks under uncertainty scenarios: A review. Simulation modelling practice and theory, 106, 102166.

[230] Hubbard, D., & Samuelson, D. A. (2009). Modeling without Measurements: How the decision analysis culture's lack of empiricism reduces its effectiveness. OR/MS Today, 36(5), 26-31.

[231] Metropolis, N., Rosenbluth, A. W., Rosenbluth, M. N., Teller, A. H., & Teller, E. (1953). Equation of state calculations by fast computing machines. The journal of chemical physics, 21(6), 1087-1092.

[232] Cover, T. M. (1999). Elements of information theory. John Wiley & Sons.

[233] Liu, J. S., Liang, F., & Wong, W. H. (2000). The multiple-try method and local optimization in Metropolis sampling. Journal of the American Statistical Association, 95(449), 121-134.

[234] Spall, J. C. (2003). Estimation via markov chain Monte Carlo. IEEE Control Systems Magazine, 23(2), 34-45.

[235] Hill, S. D., & Spall, J. C. (2019). Stationarity and convergence of the metropolis-hastings algorithm: Insights into theoretical aspects. IEEE Control Systems Magazine, 39(1), 56-67.

[236] Kolokoltsov, V. N. (2010). Feyman path integral via jump-type Markov processes for singular potentials, many particle systems and curvilinear state spaces.

[237] Del Moral, P. (2013). Mean field simulation for Monte Carlo integration. CRC press.

[238] Del Moral, P., Doucet, A., & Jasra, A. (2006). Sequential Monte Carlo samplers. Journal of the Royal Statistical Society: Series B (Statistical Methodology), 68(3), 411-436.

[239] Ripley, B. D. (2009). Stochastic simulation (Vol. 316). John Wiley & Sons.

[240] Sawilowsky, S. S. (2003). You think you've got trivials? Journal of Modern Applied Statistical Methods, 2(1), 21.

[241] Kalos, M. H., & Whitlock, P. A. (2008). Monte Carlo Method, ISBN: 978-3-527-40760-6.

[242] Jia, X., Ziegenhein, P., & Jiang, S. B. (2014). GPU-based high-performance computing for radiation therapy. Physics in Medicine & Biology, 59(4), R151.

[243] Baeurle, S. A. (2009). Multiscale modeling of polymer materials using field-theoretic methodologies: a survey about recent developments. Journal of Mathematical Chemistry, 46(2), 363-426.

[244] Möller, W., & Eckstein, W. (1984). Tridyn—A TRIM simulation code including dynamic composition changes. Nuclear Instruments and Methods in Physics Research Section B: Beam Interactions with Materials and Atoms, 2(1-3), 814-818.

[245] Golden, L. M. (1979). The effect of surface roughness on the transmission of microwave radiation through a planetary surface. Icarus, 38(3), 451-455.

[246] Mazhdrakov, M., Benov, D., & Valkanov, N. (2018). The Monte Carlo method: engineering applications. ACMO Academic Press.

[247] Panis, L. I., Nocker, L. D., Vlieger, I. D., & Torfs, R. (2001). Trends and uncertainty in air pollution impacts and external costs of Belgian passenger car traffic. International Journal of Vehicle Design, 27(1-4), 183-194.

[248] Panis, L. I., Rabl, A., De Nocker, L., & Torfs, R. (2002). Diesel or petrol? An environmental comparison hampered by uncertainty. In Proceedings of 11th International Symp. Transport and Air Pollution. Mitteilungen Institut für Verbrennungskraftmaschinen und Thermodynamik. Ed. P. Sturm, Technische Universität Graz, Austria (No. 81, pp. 48-54).

[249] Bird, G. A. (1976). Molecular gas dynamics, Clarendon.

[250] Dietrich, S., & Boyd, I. D. (1996). Scalar and parallel-optimized implementation of the direct simulation Monte Carlo method. Journal of Computational Physics, 126(2), 328-342.

[251] Nabian, M. A., & Meidani, H. (2018). Deep learning for accelerated seismic reliability analysis of transportation networks. Computer-Aided Civil and Infrastructure Engineering, 33(6), 443-458.

[252] Nabian, M. A., & Meidani, H. (2017, January). Uncertainty quantification and pca-based model reduction for parallel Monte Carlo analysis of infrastructure system reliability. In 96th Annual Meeting of the Transportation Research Board, Washington DC.

[253] Kahnert, M., & Kanngießer, F. (2020). Modelling optical properties of atmospheric black carbon aerosols. Journal of Quantitative Spectroscopy and Radiative Transfer, 244, 106849.

[254] Barka, A. A. (1992). The north Anatolian fault zone. In Annales tectonicae (Vol. 6, No. Suppl, pp. 164-195).

[255] Şengör, A. M. C., Tüysüz, O., Imren, C., Sakınç, M., Eyidoğan, H., Görür, N., & Rangin, C. (2005). The North Anatolian fault: A new look. Annu. Rev. Earth Planet. Sci., 33, 37-112.

[256] Okay, A. I., & Tüysüz, O. (1999). Tethyan sutures of northern Turkey. Geol Soc Lond Spec Publ 156: 475–515.

[257] Egeran, N., & Lahn, E. (1944). Note sur la carte sismique de la Turquie au 1: 2.400. 000. Maden Tekt. Arama Enst. Mecmuasi, 2(32), 279-289.

[258] Stein, R. S., Barka, A. A., & Dieterich, J. H. (1997). Progressive failure on the North Anatolian fault since 1939 by earthquake stress triggering. Geophysical Journal International, 128(3), 594-604.

[259] Lyakhovsky, V., & Ben-Zion, Y. (2009). Evolving geometrical and material properties of fault zones in a damage rheology model. Geochemistry, Geophysics, Geosystems, 10(11).

[260] Koulakov, I., Bindi, D., Parolai, S., Grosser, H., & Milkereit, C. (2010). Distribution of seismic velocities and attenuation in the crust beneath the North Anatolian Fault (Turkey) from local earthquake tomography. Bulletin of the Seismological Society of America, 100(1), 207-224.

[261] Saunders, P., Priestley, K., & Taymaz, T. (1998). Variations in the crustal structure beneath western Turkey. Geophysical Journal International, 134(2), 373-389.

[262] Karabulut, H., Özalaybey, S., Taymaz, T., Aktar, M., Selvi, O., & Kocaoğlu, A. (2003). A tomographic image of the shallow crustal structure in the Eastern Marmara. Geophysical Research Letters, 30(24).

[263] Bozkurt, E. (2001). Neotectonics of Turkey–a synthesis. Geodinamica acta, 14(1-3), 3-30.

[264] Siebert, L., & Simkin, T. (2002). Volcanoes of the world: An illustrated catalog of Holocene volcanoes and their eruptions, Global Volcanism Program Digital Inf. Ser., GVP-3, Smithsonian Institution., Washington, DC (Available at http://www. volcano. si. edu/world/).

[265] Berk Biryol, C., Beck, S. L., Zandt, G., & Özacar, A. A. (2011). Segmented African lithosphere beneath the Anatolian region inferred from teleseismic P-wave tomography. Geophysical Journal International, 184(3), 1037-1057.

[266] Bozdağ, E., & Trampert, J. (2008). On crustal corrections in surface wave tomography. Geophysical Journal International, 172(3), 1066-1082.

[267] Ertabaklar, H., Toz, S. O., Ozkan, A. T., Rastgeldi, S., Balcioglu, I. C., & Ozbel, Y. (2005). Serological and entomological survey in a zoonotic visceral leishmaniasis focus of North Central Anatolia, Turkey: Corum province. Acta tropica, 93(3), 239-246.

[268] Karasartova, D., Gureser, A. S., Gokce, T., Celebi, B., Yapar, D., Keskin, A., & Taylan-Ozkan, A. (2018). Bacterial and protozoal pathogens found in ticks collected from humans in Corum province of Turkey. PLoS neglected tropical diseases, 12(4), e0006395.

[269] Corum Climate Weather Averages/Turkey https://web.archive.org/web/20110430154329/-http://dmi.gov.tr/veridegerlendirme/il-ve-ilceler-istatistik.aspx?m=CORUM , Access: 2011-04-30

CURRICULUM VITAE

Ahmet Sait ALALI

[redacted]

ACADEMIC ACTIVITIES

I am planning to write some scientific articles on nuclear physics with my supervisors Prof. Dr. Fatih Kulahci.